Electrospinning and electrically forced jets. I. Stability theory

Moses M. Hohman
The James Franck Institute, University of Chicago, Chicago, Illinois 60637

Michael Shin
Department of Materials Science and Engineering, Massachusetts Institute of Technology, Cambridge, Massachusetts 02139

Gregory Rutledge
Department of Chemical Engineering, Massachusetts Institute of Technology, Cambridge, Massachusetts 02139

Michael P. Brenner[a)]
Department of Mathematics, Massachusetts Institute of Technology, Cambridge, Massachusetts 02139

(Received 15 February 2000; accepted 10 May 2001)

Electrospinning is a process in which solid fibers are produced from a polymeric fluid stream (solution or melt) delivered through a millimeter-scale nozzle. The solid fibers are notable for their very small diameters (<1 μm). Recent experiments demonstrate that an essential mechanism of electrospinning is a rapidly whipping fluid jet. This series of papers analyzes the mechanics of this whipping jet by studying the instability of an electrically forced fluid jet with increasing field strength. An asymptotic approximation of the equations of electrohydrodynamics is developed so that quantitative comparisons with experiments can be carried out. The approximation governs both long wavelength axisymmetric distortions of the jet, as well as long wavelength oscillations of the centerline of the jet. Three different instabilities are identified: the classical (axisymmetric) Rayleigh instability, and electric field induced axisymmetric and whipping instabilities. At increasing field strengths, the electrical instabilities are enhanced whereas the Rayleigh instability is suppressed. Which instability dominates depends strongly on the surface charge density and radius of the jet. The physical mechanisms for the instability are discussed in the various possible limits. © *2001 American Institute of Physics.* [DOI: 10.1063/1.1383791]

I. INTRODUCTION

Electrospinning is a process that produces a highly impermeable, nonwoven fabric of submicron fibers by pushing a millimeter diameter liquid jet through a nozzle with an electric field.[1–7] In the conventional view,[1] electrostatic charging of the fluid at the tip of the nozzle results in the formation of the well known Taylor cone, from the apex of which a single fluid jet is ejected. As the jet accelerates and thins in the electric field, radial charge repulsion results in splitting of the primary jet into multiple filaments, in a process known as ''splaying.''[1] In this view the final fiber size is determined primarily by the number of subsidiary jets formed.

We have recently demonstrated[8] that an essential mechanism in electrospinning involves a rapidly whipping fluid jet. The whipping of the jet is so rapid under normal conditions that a long exposure photograph (e.g., >1 ms) gives the *envelope* of the jet the appearance of splaying subfilaments. A systematic exploration of the parameter space of electrospinning (as a function of the applied electric field, volume flux, and liquid properties) revealed that for PEO/water solutions, the onset of electrospinning always corresponds with the whipping of the jet.

The goal of this series of papers is to develop a theoretical framework for understanding the physical mechanisms of electrospinning, and to provide a way of quantitatively predicting the parameter regimes where it occurs. The theory consists of two components: a stability analysis of a cylinder of fluid with a static charge density in an external electric field, and a theory for how these properties vary along the jet as it thins away from the nozzle. By analyzing various instabilities of the jet, we show that it is possible to make predictions for the onset of electrospinning that quantitatively agree with experiment.

The formalism we describe here also has application to electrospraying[9–14] for which it has long been known that there are *many* different operating modes, originally documented by Cloupeau and Prunet-Foch.[15,16] A recent review article[17] classifies the different modes as (a) dripping, when spherical droplets detach directly from the Taylor cone; (b) spindle mode, in which the jet is elongated into a thin filament before it breaks into droplets; (c) oscillating jet mode, in which drops are emitted from a twisted jet attached to the nozzle, and the (d) the precession mode, in which a rapidly whipping jet is emitted from the nozzle, before it breaks into droplets. The last two modes are qualitatively similar to the whipping mode we find in electrospinning.

[a)]Author to whom all correspondence should be addressed. Present address: Division of Engineering and Applied Sciences, Harvard University, Cambridge, Massachusetts 02138. Electronic mail: brenner@deas.harvard.edu

A series of papers in the electrospraying community has focused on the properties of the jet of fluid emitted from the Taylor cone.[18–25] These papers demonstrate that (in certain regimes of parameter space) the current–voltage relationship[26] can be rationalized using the asymptotic properties of a thinning fluid jet, assuming the jet remains a continuous stream. The types of calculations described in the present papers would allow these jet solutions to be extended to predict which operating mode occurs in electrospraying as a function of parameters.

The idea of the analysis is straightforward: first we will develop a stability theory for a cylinder of a fluid (with fixed surface tension, conductivity, viscosity, dielectric constants, etc.) in an axial applied electric field (i.e., pointing along the axis of the jet) with an arbitrary charge density. We then apply this stability analysis to the relevant solution for the jet's shape, charge density, etc. The predicted mode of instability that is excited turns out to depend on the fluid properties and the process variables (e.g., applied flow rate and electric field) in a manner that can be predicted quantitatively. As will be seen in a companion paper,[8] treatment of the fluid as Newtonian is adequate for the range of fluids and operating conditions explored here.

The basic principles for dealing with electrified fluids were developed in a series of papers written by Taylor in the 1960s.[27–30] Taylor discovered that it is impossible to account for most electrical phenomena involving moving fluids under the seemingly reasonable assumptions that the fluid is either a perfect dielectric or a perfect conductor. The reason is that any perfect dielectric still contains a nonzero free charge density. Although this charge density might be small enough to ignore bulk conduction effects, the charge will typically live on *interfaces* between fluids. If there is also a nonzero electric field tangent to the interface then there will be a nonzero tangential stress on the interface. The only possible force that can balance a tangential stress is viscous; hence, under these conditions the fluid will necessarily be in motion. This idea has become known as the ''leaky dielectric model'' for electrically driven fluids. Its consequences have been successfully compared to experiments on neutrally buoyant drops elongated by electric fields. A detailed discussion and derivation of the assumptions behind the model are described in the recent review by Saville.[31]

Despite the general acceptance of the leaky dielectric model, a review of the literature reveals that no theory for the destabilization of an electrically forced jet has ever been quantitatively compared with experiments. The linear stability analysis of an uncharged jet in an electric field was performed by Saville in the early 1970's.[32,33] The reason that quantitative tests have not been undertaken are partially explained in Saville's[33] original papers; the stability analysis for a finite conductivity cylinder in a tangential electric field neglects two important effects, the presence of surface charge on the jet and the thinning of the radius. Similarly, the analysis[34,35] of the stability of a jet with a constant surface charge density assumed infinite conductivity, zero tangential electric field, and a constant radius jet. Saville's analyses predict qualitative characteristics consistent with the experiments—most notably the presence of both an axisymmetric instability and an oscillatory ''whipping'' instability of the centerline of the jet; however, the quantitative characteristics of these instabilities disagree strongly with experiments. As an example, a water jet with a radius of order that used in Taylor's 1969 experiments[29] is predicted to have a most unstable wavelength between 1/27–1/2 of a jet radius,[33] in direct contradiction with the pronounced long wavelength instability found in the experiments. Recent work[36,37] has included surface charge in special limits, although the aforementioned discrepancies with experiments remain unresolved.

The organization of this paper is as follows: in Sec. II we revisit the stability of an axisymmetric jet. We derive an asymptotic model for the dynamics of the jet by modifying previous theories of nonelectrical[38] and dielectric[39] jets to include free charges. The linear dispersion relations extend those previously obtained in the nonelectrical, dielectric and other special parameter limits. The simplicity of the formulas allows straightforward physical interpretation of the two main instability modes; the Rayleigh mode, which is the electrical counterpart of the surface tension driven Rayleigh instability, and a conducting mode, which involves a purely electrical competition between free charge and the electric fields. At high fields/charge densities the classical Rayleigh instability is completely stabilized and all instabilities are purely electrical; surface tension does not affect the stability characteristics of a strongly forced electrical jet.

Section III develops a theory for the whipping instability of the jet, which proceeds from a view of the jet as a fiber forced by electrical and surface stresses. We apply the formalism for deriving the equations of elasticity[40] to find a dynamical equation for the fiber; by properly computing the electrical stresses, we recover previous stability results for the bending of the fiber. Because of the simplicity of this theory, it is again easy to develop a simple physical interpretation for the various mechanisms causing instability, and also to extend previous stability results to the parameter regimes important in the experiments (i.e., finite viscosity, finite conductivity, and finite surface charge).

Section IV examines the competition between the two electrical instabilities and describes which happens first. We find that in the absence of surface charge the axisymmetric mode is more unstable than the whipping mode, so that an experiment without surface charge should see a predominant axisymmetric instability. Experiments on electrically forced jets dating back to Taylor[29] observe predominantly a whipping jet; this is explained by the demonstration that when surface charge is included in the stability analysis the relative stability of these two modes can change, so that whipping can be more unstable. This is indeed what occurs when reasonable estimates for the surface charge density in a typical electrospinning experiment is used.

The second paper in this series applies these results to explain quantitatively our experiments on electrospinning, and also shows how these results can be useful for understanding the origin of the different modes of electrospraying.

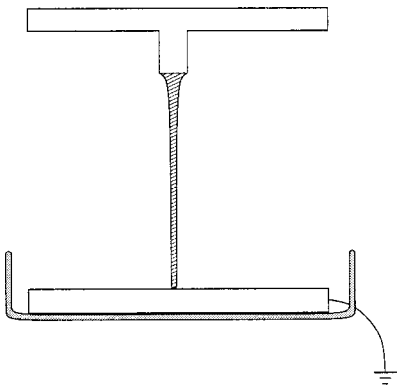

FIG. 1. Experimental setup.

II. ASYMPTOTIC THEORY OF AXISYMMETRIC JETS

We now define and develop the physical model of the experimental system shown in Fig. 1. A thin metal tube guides the fluid perpendicular to and through the center of a broad capacitor plate and opens into free space. The tube opening protrudes slightly from the surface of the plate. The jet then flows out of the tube and downward (with gravity) between the top plate and another identical plate below it. The bottom plate sits in a glass collecting dish. The two capacitor plates are positioned perpendicular to the flow so that the externally imposed electric field is very nearly uniform and axial in the region of the jet. The experimentally adjustable parameters (aside from material parameters of the jet fluid) are the electrostatic potential difference between the plates, V, the separation between the plates, d, and the constant rate at which fluid flows from the tube, Q. We will denote the constant field far from the nozzle as E_∞; later in the paper, it will become apparent that the fringe fields around the nozzle are also important.

The external fluid is air, which is assumed to have no effect on the jet except to provide a uniform external pressure. This assumption holds until the jet becomes so thin that air drag and air currents become important. The internal fluid is assumed to be Newtonian and incompressible. This assumption holds for dilute solutions under low shear and in the absence of high degrees of extension. The fluid parameters for the internal fluid are: conductivity, K, dielectric constant, ϵ, mass density, ρ, and kinematic viscosity, ν. The dynamic viscosity is $\mu=\rho\nu$. The coefficient of interfacial tension between the fluid and the air is γ. The dielectric constant of the air is assumed to be $\bar{\epsilon}$. In general, overbarred quantities will refer to the region *outside* the jet.

To proceed, we must consider the relaxation of free charge in the system. The classical relaxation time is, in Gaussian units,

$$\tau_e=\frac{\epsilon}{4\pi K}.$$

This is the timescale for the *local* relaxation of bulk charge density within a conducting medium. This process is usually much faster than the global equilibration of charge on the surface of a conductor. For example, for copper $\tau_e \approx 10^{-19}$ s, whereas it is common experience that it takes much longer for electrical equilibration to occur through a copper wire. The reason for this difference is that the global relaxation of charge occurs via charge neutral currents in the bulk of a medium, which depend in general on the geometry of the material in question (e.g., in a copper wire the RC constant is the relevant time for relaxing imposed potential differences). This point is especially important to the study of electrospinning and electrospraying; τ_e is sometimes employed without taking the care to make this important distinction.

We will assume throughout this paper that free charge in the bulk has ample time to relax to its equilibrium value (i.e., that τ_e is irrelevant), so that all free charge resides on the surface of the jet. In a typical experiment a current, I, flows through the jet due to its bulk conductivity and the advection of charge along the surface. This current is experimentally determined to be a function of the fluid parameters, Q,E_∞, and the geometry of the nozzle.

A. Derivation of axisymmetric equations

The equations for the jet follow from Newton's Law and the conservation laws it obeys, namely, conservation of mass and conservation of charge. Because of viscous dissipation and external forcing by both gravity and the electric field, the isolated system of the jet does not conserve energy or momentum. We also employ Coulomb's integral equation for the electric field.

The first step in the derivation assumes that the jet is a long, slender object and then uses a perturbative expansion in the aspect ratio. This idea has been recently used in modeling jets without electric fields (for a comprehensive review, see Ref. 38). This approximation method rests on expanding the relevant three-dimensional fields (axial velocity, v_z, radial velocity, v_r, radial electric field, E_r, and axial electric field, E_z) in a Taylor series in r, e.g.,

$$v_z(z,r)=v_0(z)+v_1(z)r+v_2(z)r^2+\cdots. \tag{1}$$

We then substitute these expansions into the full three-dimensional equations and keep only leading order terms. This leads to a set of equations that is actually rather intuitive. The conservation of mass equation is

$$\partial_t(\pi h^2)+\partial_z(\pi h^2 v)=0, \tag{2}$$

where $h(z)$ is the radius of the jet at axial coordinate z and $v(z)$ is the axial velocity, which to leading order is constant across the jet cross section [i.e., Eq. (1) with $v_0=v$].

Similarly, conservation of charge becomes

$$\partial_t(2\pi h\sigma)+\partial_z(2\pi h\sigma v+\pi h^2 KE)=0, \tag{3}$$

where $\sigma(z)$ is the surface charge density, and $E(z)$ is the electric field in the axial direction. There is now an extra component to the current besides advection due to bulk conduction in the fluid.

Momentum balance, or the Navier–Stokes equation, becomes

$$\partial_t v+\partial_z\left(\frac{v^2}{2}\right)=-\frac{1}{\rho}\partial_z p+g+\frac{2\sigma E}{\rho h}+\frac{3\nu}{h^2}\partial_z(h^2\partial_z v), \tag{4}$$

where $p(z)$ is the internal pressure of the fluid. The hydrodynamic terms are familiar.[38] In addition there are electro-

TABLE I. Table of symbols used in this work.

Q	Volume flux
I	Current
E_∞	Applied electric field
ϵ	Fluid dielectric constant
$\overline{\epsilon}$	Air dielectric constant
K	Liquid conductivity
ν	Kinematic viscosity
ρ	Liquid density
γ	Surface tension
μ	Dynamic viscosity
g	Gravitational acceleration
h	Radius of jet
σ	Surface charge density
V	Voltage drop between the capacitor plates
d	Distance between capacitor plates
E	Electric field parallel to axis of jet
v	Fluid velocity parallel to axis of jet
p	Pressure in the fluid
λ	Linear charge density along the jet
$\mathbf{P}$	Dipole density along the jet
β	$\epsilon/\overline{\epsilon}-1$
$\mathbf{M}$	Internal moment of bent fiber
$\mathbf{N}$	External torque on bent fiber
$\mathbf{K}$	External force on bent fiber
$\mathbf{F}$	Tension in bent fiber
$\mathbf{r}$	Coordinate of centerline of bent fiber
σ_D	Dipolar component of free charge density
K^*	Dimensionless conductivity
ν^*	Dimensionless viscosity
Ω_0	Dimensionless external field strength
σ_0	Dimensionless background free charge density

static terms in the pressure and a tangential stress term, $2\sigma E/\rho h$. The latter accelerates the jet due to the presence of both surface charge and a tangential component of the electric field at the jet surface.

The pressure is

$$p=\gamma\kappa-\frac{\epsilon-\overline{\epsilon}}{8\pi}E^2-\frac{2\pi}{\overline{\epsilon}}\sigma^2, \tag{5}$$

where κ is twice the mean curvature of the interface ($\kappa=1/R_1+1/R_2$, where R_1 and R_2 are the principal radii of curvature). The electrostatic term proportional to E^2 is the difference across the interface of the energy density of the field ($\epsilon E^2/8\pi$) if we neglect contributions from the asymptotically small E_r (the radial field inside the jet). The term proportional to σ^2 is just the radial self-repulsion of the free charges on the surface. (This term can also be interpreted as the difference in the energy density in the radial electric field, where again we neglect terms proportional to E_r.) When we evaluate R_1 and R_2 we obtain $R_1\approx 1/h$ and $R_2\approx -h''$, where the prime refers to differentiation in z. h'' is higher order than $1/h$, but it is also the stabilizing part of surface tension, so in certain cases we retain this term (Table I).

The one important difference between the derivation of this equation and that for nonelectric jets is that an additional assumption must be made for the expansion in Eq. (1) to be asymptotically valid; namely, the tangential stress caused by the electric field σE must be much smaller than the *radial* viscous stress, $\mu v/h$. Whether or not this is true in a given situation needs to be determined *a posteriori*; if a solution computed with the model would ever violate this assumption the solution would break down. In every case we have studied the assumption has held uniformly in both space and time.

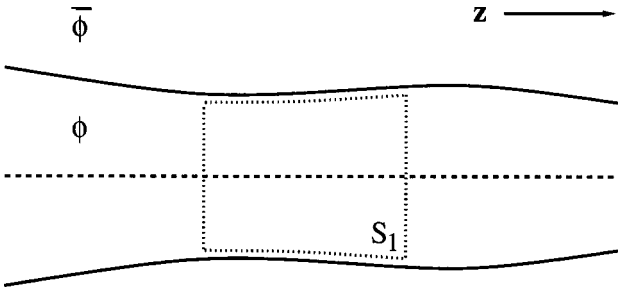

FIG. 2. Gaussian surface, S_1, lies just inside the interface.

Now we turn to the derivation of the equation for the electric field. [The philosophy of this derivation was inspired by a comment of E. J. Hinch. See the Appendix of Ref. 39.] The electric field outside the slender jet can be written down as if it were due to an effective linear charge density (incorporating both free charge and polarization charge effects) of charge $\lambda(z)$ along the z-axis. To find this linear charge density, we perform a customary Gauss' law argument twice. The first time we pick a cylindrical Gaussian surface, S_1, coaxial with the jet, of length dz and radius just less than $h(z)$ (see Fig. 2). This surface contains no charge (and no effective charge, since we are inside the cylinder). Thus, denoting E_r and E_z the radial and axial components of the field inside the jet evaluated at the jet surface, we obtain

$$0=\oint_{S_1}\mathbf{E}\cdot\hat{\mathbf{n}}dA=[(\pi h^2E_z)'+2\pi hE_r]dz,$$

so that

$$2\pi hE_r=-(\pi h^2E_z)'.$$

Now we pick a new Gaussian surface, S_2, in the same position as S_1 with the same length but a radius just bigger than $h(z)$ (see Fig. 3). Since this surface surrounds the entire jet volume, it contains some effective charge, in particular it contains $\lambda(z)dz$. Denoting fields outside the jet with an overbar,

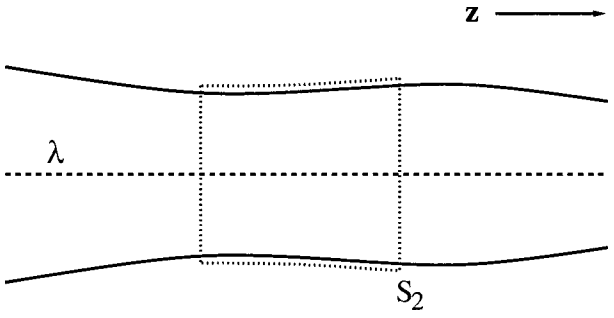

FIG. 3. Gaussian surface, S_2, lies just outside the interface and thus contains charge.

$$4\pi\lambda(z)dz = \oint_{S_2} \mathbf{E}\cdot\hat{\mathbf{n}}dA = [(\pi h^2 E_z)' + 2\pi h\overline{E_r}]dz. \quad (6)$$

For a slender jet we know that

$$\overline{E_r} \approx \overline{E_n} = \frac{\epsilon}{\overline{\epsilon}}E_n + \frac{4\pi\sigma}{\overline{\epsilon}}. \quad (7)$$

So,

$$\lambda(z) = -\frac{\beta}{4}(h^2 E_z)' + \frac{2\pi h\sigma}{\overline{\epsilon}}, \quad (8)$$

where

$$\beta = \frac{\epsilon}{\overline{\epsilon}} - 1.$$

Now we can plug this effective linear charge density into Coulomb's Law for the electrostatic potential outside the jet. We will assume that λ varies over a length scale, L, much larger than the radius, and approximate the integral in that case,

$$\begin{aligned}\overline{\Phi}(z,r) &= \overline{\Phi}_\infty + \int dz' \frac{\lambda(z')}{\sqrt{(z-z')^2+r^2}} \\ &\approx \overline{\Phi}_\infty + \lambda(z)\int dz' \frac{1}{\sqrt{(z-z')^2+r^2}} \\ &\approx \overline{\Phi}_\infty - 2\ln\frac{r}{L}\lambda(z) \\ &= \overline{\Phi}_\infty + \ln\frac{r}{L}\left(\frac{\beta}{2}(h^2E_z)' - \frac{4\pi}{\epsilon}h\sigma\right). \end{aligned} \quad (9)$$

Elementary electrostatics tells us that the tangential component of the electric field is continuous across the interface, so $\tilde{E}_z \approx \overline{E_t} = E_t \approx E_z$. This yields a single equation for the tangential field inside the jet,

$$E - \ln\left(\frac{1}{\chi}\right)\left[\frac{\beta}{2}(h^2E)'' - \frac{4\pi}{\overline{\epsilon}}(h\sigma)'\right] = E_\infty, \quad (10)$$

where $E = E_z$. The variable χ^{-1} is the local aspect ratio, which is assumed the be small.

If the fluid takes a conical shape, there is only one possible choice for χ, the slope of the cone. This fact allowed[39] us to calculate asymptotic equilibrium cone angles at the tips of electrified, perfect dielectric fluid drops that agreed very well with the exact theory for infinite cones. This simplification also will occur subsequently for the sinusoidally perturbed, perfect cylinders of linear stability analysis, where χ must be proportional to the wave number k of the perturbation. This fact will allow us to calculate dispersion relations for electrified jets that agree well with previous results (e.g., of Saville), which are derived from the full three-dimensional equations. For generic situations where χ is less easily defined, we must either disregard the factor of $\ln(1/x)$, since it is a logarithm and will not vary too much, or use some local estimate. To achieve quantitative agreement with experiments near a nozzle, it will turn out that it is necessary to employ the full integral equation for the field caused by both $\lambda(z)$, and its image charges. (See the second paper in this series.)

The aforederived equations are nondimensionalized by choosing a length scale r_0 (e.g., the nozzle diameter), a time scale $t_0 = \sqrt{\rho r_0^3/\gamma}$, an electric field strength $E_0 = \sqrt{\gamma/[(\epsilon - \overline{\epsilon})r_0]}$ and a surface charge density $\sqrt{\gamma\overline{\epsilon}/r_0}$. We denote the dimensionless asymptotic field $\Omega_0 = E_\infty/E_0$. (For ease of comparison, we note that the relationship between our Ω_0 and Saville's parameter E is $\Omega_0^2 = 4\pi\beta E$.) Four dimensionless parameters characterize the material properties of the jet: $\beta = \epsilon/\overline{\epsilon} - 1$, the dimensionless viscosity $\nu^* = \sqrt{l_\nu/r_0}$ (with the viscous scale $l_\nu = \rho\nu^2/(\gamma)$), the dimensionless gravity $g^* = g\rho r_0^2/\gamma$, and the dimensionless conductivity $K^* = K\sqrt{r_0^3\rho/(\gamma\beta)}$. Typical values of the viscous length scale are $l_\nu = 100$ Å for water, and $l_\nu = 1$ cm for glycerol. Whether viscous stresses are important depends on the ratio of this length scale to the jet radius. A conductivity of 1 μS/s (at the upper range for our experiments) corresponds to a relaxation time of ≈ 1 μs; K^* compares this to a capillary time for a 0.1 mm jet of about 10^{-3} s. Hence, when the jet is thick, it is a very good conductor indeed.

The nondimensional equations are then

$$\partial_t(h^2) + (h^2 v)' = 0, \quad (11)$$

$$\partial_t(\sigma h) + \left(\sigma h v + \frac{K^*}{2}h^2 E\right)' = 0, \quad (12)$$

$$\partial_t v + v v' = -\left(\frac{1}{h} - h'' - \frac{E^2}{8\pi} - 2\pi\sigma^2\right)' + \frac{2\sigma E}{\sqrt{\beta}h} + g^* + \frac{3\nu^*}{h^2}(h^2 v')', \quad (13)$$

$$E - \ln\frac{1}{\chi}\left[\frac{\beta}{2}(h^2E)'' - 4\pi\sqrt{\beta}(h\sigma)'\right] = \Omega_0. \quad (14)$$

B. Stability analysis

Now we present and discuss the local linear stability analysis of axisymmetric perturbations to an electrified jet. There are three equilibrium states around which one could imagine perturbing (see Fig. 4); there are two perfectly cylindrical states, one in which there is an applied field but no initial surface charge density, and another [Fig. 4(b)] with no applied field but an initial charge density (so that the field inside is zero, initially). Neither of these are relevant for our electrospinning experiments. A more realistic state for experiments thins due to the tangential stress at the interface from the interaction between the static surface charge density and the tangential electric field. We remark that there are experimental configurations where Fig. 4(b) is the appropriate limit; in particular in the "point plate" geometry, the electric field decays away from the nozzle. Far enough downstream, the surface charge density can bet the external field. This is the geometry used in most electrospraying experiments.[41]

The third state is the most general of the three; as long as the wavelength of the perturbation is much smaller than the characteristic decay length of the jet, the stability characteristics can be approximated by considering perturbations to a

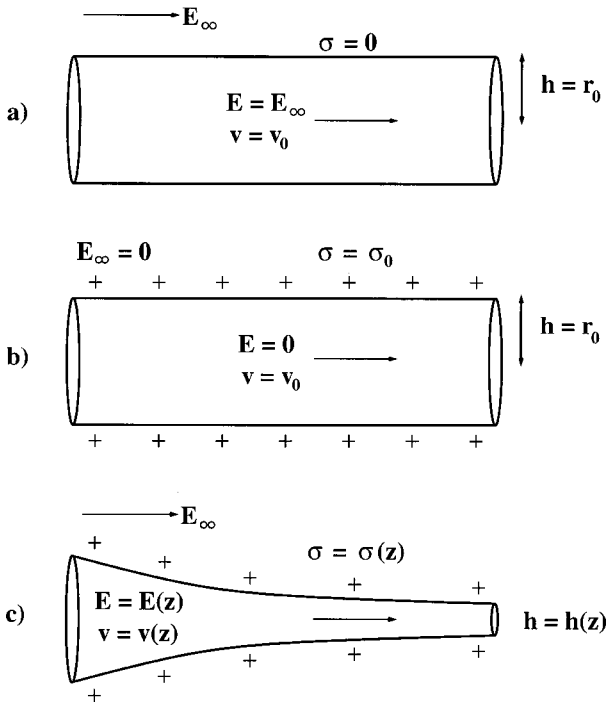

FIG. 4. Jet equilibria around which linear stability may be performed. (a) and (b) were approached by Saville, (c) is more realistic for comparing with experiments.

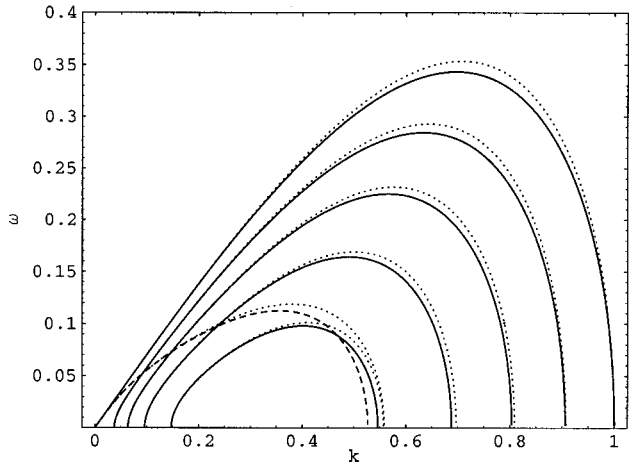

FIG. 5. Comparison of Saville's (Ref. 33) dispersion relation for a zero viscosity fluid as a function of field strength, for $\beta=77$. The solid lines are Saville's results for infinite conductivity, with field strengths, $\Omega_0^2=0,0.97,1.93,2.90,3.8$ from the uppermost to the lowermost, respectively. The dashed line is for zero conductivity and $\Omega_0^2=4.83$. The dotted lines are from Eq. (19).

charged cylinder of constant radius. Since this state encompasses the other two we will consider it alone in the following. Because of the simplicity of the model, it will be possible to understand the stability of the jet as a function of all fluid and electrical parameters.

To determine the linear stability, we solve for the dynamics of small perturbations to the constant radius, electric field and charge density solution using the ansatz $h=1+h_\epsilon e^{\omega t+ikx}$, $v=0+v_\epsilon e^{\omega t+ikx}$, $E=\Omega_0+e_\epsilon e^{\omega t+ikx}$, and $\sigma=\sigma_0+\sigma_\epsilon e^{\omega t+ikx}$, where $h_\epsilon, v_\epsilon, e_\epsilon, \sigma_\epsilon$ are assumed to be small. Substituting this into Eqs. (11)–(14) yields

$$2\omega h_\epsilon + ikv_\epsilon = 0, \tag{15}$$

$$\omega\sigma_\epsilon + \frac{K^*}{2}(2\Omega_0 h_\epsilon + e_\epsilon)ik + ik\sigma_0 v_\epsilon = 0, \tag{16}$$

$$\omega v_\epsilon = (ik - ik^3)h_\epsilon + \frac{\Omega_0}{4\pi}ike_\epsilon + 4\pi ik\sigma_0\sigma_\epsilon + \frac{2\Omega_0}{\sqrt{\beta}}\sigma_\epsilon + \frac{2\sigma_0 e_\epsilon}{\sqrt{\beta}} - 2\frac{\sigma_0\Omega_0}{\sqrt{\beta}}h_\epsilon - 3\nu^* k^2 v_\epsilon = 0, \tag{17}$$

$$\frac{\delta}{2}e_\epsilon + \Lambda\Omega_0 h_\epsilon + \frac{4\pi i\Lambda}{\sqrt{\beta}k}\sigma_\epsilon \frac{4\pi i\lambda\sigma_0}{\sqrt{\beta}k}h_\epsilon = 0, \tag{18}$$

where $\Lambda=\beta\ln(1/\chi)k^2$, $\delta=2+\Lambda$. These equations have a nontrivial solution only if the determinant of the coefficient matrix vanishes; this requirement yields the dispersion relation,

$$\omega^3 + \omega^2\left[\frac{4\pi K^*\Lambda}{\delta\sqrt{\beta}} + 3\nu^* k^2\right] + \omega\left[3\nu^* k^2\frac{4\pi K^*\Lambda}{\delta\sqrt{\beta}} + \frac{k^2}{2}(k^2-1) + 2\pi\sigma_0^2 k^2\left(\frac{8\mathcal{L}}{\delta}-1\right) + \frac{\Lambda}{\delta}\frac{\Omega_0^2}{4\pi}k^2\right] + \frac{4\pi K^*\Lambda}{\delta\sqrt{\beta}}\left[\frac{k^2}{2}(k^2-1) + 2\pi\sigma_0^2 k^2 + \frac{\delta}{\Lambda}\frac{\Omega_0^2}{4\pi}k^2 + \frac{E_0\sigma_0}{\sqrt{\beta}}ik\left(\frac{1}{\mathcal{L}}-4\right)\right] = 0, \tag{19}$$

where $\mathcal{L}=\ln(1/\chi)$. Since this equation is cubic, there will in general be three different branches of the dispersion relation; an instability occurs if any of these branches has $\mathrm{Re}\,\omega>0$. Although Eq. (19) is complicated, we wish to emphasize that (a) it is vastly simpler than dispersion relations that have previously been derived for this problem; for example, the analogous formulas in Saville[33] (for the special case of a jet with no net charge density) involves solving a cubic equation with coefficients that involve determinants of matrices of Bessel functions, whose *arguments* include the growth rate, ω. Mestel[37] has considered the stability of a jet in a field with nonzero surface charge density in the very viscous limit (liquid density $\rho\to 0$). Describing the calculation, he states "the algebra is exceedingly nasty, even with the help of *Mathematica*." (b) Equation (19) works for arbitrary values of the conductivity, dielectric constant, viscosity, and field strength, as long as the condition that the tangential electrical stress is smaller than the radial viscous stress is satisfied. Technically, the formula is asymptotically correct in the $k\to 0$ limit. It therefore extends the previous results to regimes which have heretofore not been examined; importantly, this includes the regime of most experiments.

To demonstrate the asymptotic validity of these formulas, we first compare the results of different limits of Eq. (19)

with those of previous authors. First, we compare to Saville's results: Figs. 5 and 6 show comparisons in two of the three parameter regimes reported in Ref. 33. [We note that there is one small freedom in our dispersion relation, namely, the relationship between the local aspect ratio of the jet χ^{-1} and the wave number k. Clearly $\chi^{-1}=Ak$. We determine A by expanding Saville's dispersion relation [Eq. (32) of Ref. 33] in the low viscosity limit at low k, and then demanding that the value of A in his calculation agrees with ours. This implies that $A=\exp(\gamma)/2=0.89...$, where γ is Euler's gamma. We use this value of A in all subsequent comparisons, so that A is independent of all fluid and control parameters.]

Figure 5 compares the zero viscosity and infinite conductivity limit from Eq. (19) (dotted lines) to Saville's results (solid lines), for several values of the applied field, Ω_0. In this regime, increasing the applied electric field stabilizes the jet. The agreement is excellent, and is exact at low k. Also shown in this figure is a comparison in the zero conductivity limit. The agreement between Saville's relation (the dashed line) and Eq. (19) is exact at low k.

The dispersion relation (19) also yields a simple analytic expression that gives the growth rate in the infinite conductivity, zero viscosity limit,

$$\omega=k\sqrt{\frac{1}{2}(1-k^2)-2\pi\sigma_0^2-\frac{\Omega_0^2}{4\pi}\left(1+\frac{2}{\beta k^2\ln(Ak)}+\frac{\Omega_0\sigma_0 i}{\sqrt{\beta}k}\right)}. \tag{20}$$

When σ_0,Ω_0 are zero, this formula gives the classical Rayleigh instability. When the field Ω_0 is increased, the Rayleigh instability is suppressed. At a critical field strength, the instability completely goes away. In the limit of large β with $\sigma_0=0$, this critical field is given by the formula

$$\Omega_{0\,\mathrm{crit}}\approx\sqrt{2\pi}=2.5\cdots. \tag{21}$$

In dimensional units, the criterion is

$$(\epsilon-\overline{\epsilon})E_\infty^2=\frac{2\pi\gamma}{r_0}. \tag{22}$$

This formula has a simple physical interpretation; when the electrical pressure per unit length of the jet exceeds the surface tension pressure per unit length, the instability is suppressed. It turns out that this critical field strength has the same value even when the conductivity or viscosity is finite. This critical field is comparable to typical experimental values: for a 1 mm jet of water in an electric field of 2 kV/cm, the nondimensional applied field, $\Omega_0\approx2$, so that the local field in the thinning jet is close to the critical value. For a 10 μm jet, Ω_0 is approximately 0.2. The consequence of this is that it demonstrates that at high fields neither surface tension nor the classical Rayleigh instability is important for the breakup of electrified jets until the jet becomes very thin.

Figure 6 shows a comparison at finite conductivity, so that the electrical relaxation time ϵ/K is finite, and infinite viscosity. In this limit, the growth rate, ω, can become complex, corresponding to oscillatory modes. Figure 6 shows the growing modes for three different values of $\tau=(\epsilon/K)\times(\gamma/(r_0\mu))$ at an imposed electric field $\Omega_0=1.56$. The solid lines and the dashed lines are Saville's results; the dashed lines represent oscillatory modes, which are unstable at small r. Our dispersion relation is superimposed on Saville's with no discernable difference.

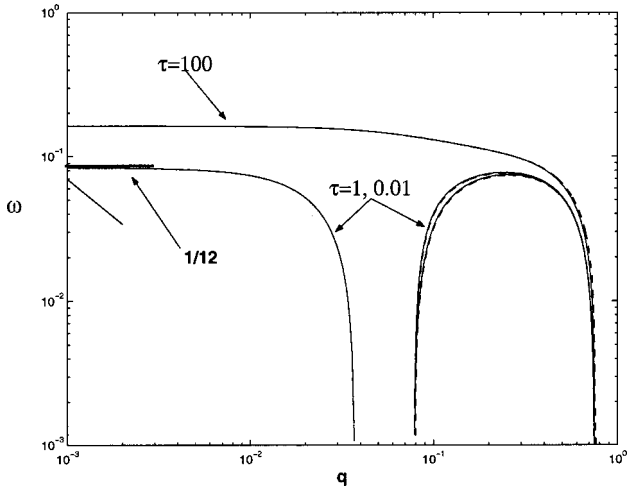

FIG. 6. Comparison of Saville's (Ref. 34) dispersion relation for an infinite viscosity fluid with different finite electrical relaxation time $\tau=\epsilon/K\gamma/(\mu r_0)=0.01$, 1, and 100, respectively. The rightmost lines show nonoscillatory modes (i.e., Im $\omega=0$) and the leftmost lines show oscillatory modes. The result from the dispersion relation [Eq. (19)] (dashed lines) is superimposed on Saville's solution (solid lines) with no discernable difference.

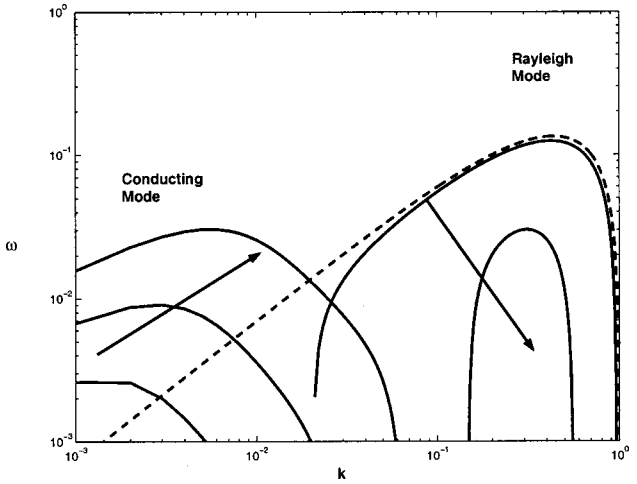

FIG. 7. Field dependence of the instability growth rate ω for a fluid with $\nu=140$ cP, $\gamma=65$ dyn/cm, conductivity $K=5.8\mu$ and $\epsilon=78$. As the field is increased (direction indicated by arrows) the ''Raleigh mode'' is suppressed and the conducting mode becomes dominant.

These plots demonstrate that the asymptotic theory reproduces the previous results. Before proceeding further, it is pedagogical to first examine how the growth rate varies with electric field, in order to develop intuition for how the field interacts with the fluid. Figure 7 shows the dependence of ω on k and E_∞ for a fluid with $\nu=140$ cP, $\gamma=65$ dyn/cm, conductivity $K=5.8\,\mu$S, and $\epsilon=78$. The arrows indicate what happens when the external field increases. The zero field-result is the dashed curve; as the field increases this ''Rayleigh mode'' has a positive growth rate for a smaller and smaller range of wave vectors. At the critical field the Rayleigh mode is completely suppressed. However, the jet is still unstable, because a new ''conducting mode'' becomes larger and larger as the field is increased. This conducting mode is oscillatory (the imaginary part of its growth rate is nonzero), and is the root cause of the oscillatory growth rates observed by Saville.[33] (We will see below that when surface charge is included, both the Rayleigh mode and the conducting mode are modified in important ways; however, the basic distinction between them still exists, and is important for interpreting experiments.[42])

The physics of this conducting mode is a consequence of the interaction of the electric field with the surface charge on the jet; surface tension is an irrelevant parameter for this mode. The mechanism for the instability is that a modulation in the radius of the jet induces a modulation in the surface charge density (which is induced because at low frequencies the charges try to cancel out the field inside the jet). The nonzero surface charge results in a tangential stress, which accelerates the liquid and causes instability. The oscillatory character of the instability results because the timescale for the fluid response is different than the timescale for the axial surface charge rearrangements. In contrast to the ordinary Rayleigh instability (in an electric field), the conducting mode is *always* unstable at long wavelengths (low k) when the applied field is nonzero. The maximum growth rate of the conducting mode scales like $\omega_{\text{conduct}}\sim\Omega_0\sqrt{K^*}$.

An important consequence of these results (cf. also Saville[34]) is that they imply that models for electrically forced jets which either assume perfect conductivity or a perfect dielectric are qualitatively incorrect. The existence of the conducting mode occurs because when the conductivity is finite the equation for the growth rate is cubic, so that there is an extra root. For models without finite conductivity this mode does not exist; hence such models have no chance at capturing the physics in this regime.

As a final check on the stability formulas, we note that in the limit where the surface charge is nonzero but the external electric field vanishes, our results also reduce to those found previously in the appropriate limits. As an example, Saville considered the stability of a perfectly conducting, charged cylinder in the viscous limit without a tangential electric field. His dispersion relation gives $\omega=\gamma(6r_0\rho\nu)^{-1}(1-4\pi r_0\sigma^2\gamma\epsilon)^{-1}$ (with σ the charge density on the cylinder). This agrees exactly with the prediction of Eq. (19) in the $k\to 0$ limit.

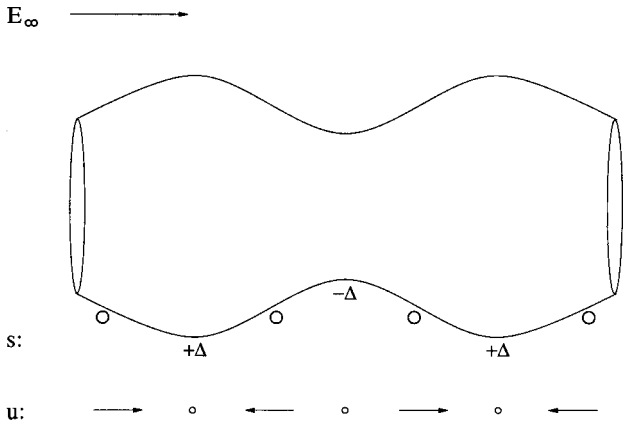

FIG. 8. Physical picture of an unstable perfect dielectric jet; the perturbation in the velocity pushes surface charge into the bulging regions.

C. Physical intuition with surface charge

The presence of surface charge modifies the characteristics of both the Rayleigh and the conducting modes in a fashion that is not (at first glance) intuitive. To explain how this works, we first present further description of how the various instabilities described above operate (to aid intuition), and then explain how a static surface charge changes the mechanics.

1. Perfect dielectrics

It will be helpful for our intuitive exploration to discuss the forms of the perturbation of the velocity, charge density, and electric field in terms of the perturbation to the radius, h_ϵ. These follow from Eqs. (15)–(18). For a perfect dielectric, the equations reduce to

$$v_\epsilon=\frac{2i\omega}{k}h_\epsilon, \tag{23}$$

$$\sigma_\epsilon=2\sigma_0 h_\epsilon, \tag{24}$$

$$e_\epsilon=-\left(\frac{2\Lambda}{\delta}\Omega_0+ik\frac{24\pi\sqrt{\beta}}{\delta}\sigma_0\right)h_\epsilon, \tag{25}$$

with the momentum response given by (17).

The velocity perturbation, v_ϵ, is $\pi/2$ out of phase with the radius perturbation, and for a growing mode it pushes fluid into the bulging regions and draws fluid from the narrowing regions. This motion pushes not only fluid but surface charge as well, so surface charge piles up in the bulging regions as well as fluid, hence σ_ϵ is in phase with h_ϵ (see Fig. 8). The electric field response is more complicated. The part of e_ϵ proportional to Ω_0 is in phase with h_ϵ; it is due to the polarization of the fluid resisting the penetration of the external field, Ω_0, into the bulging regions (hence it is negative, see Fig. 9). The part proportional to σ_0 is the electric field due to the perturbed charge density σ_ϵ, and is therefore $\pi/2$ out of phase with h_ϵ.

If σ_0 is nonzero, then there are two additional competing effects. The pressure due to the self-repulsion of charge ($p\propto\sigma^2$) destabilizes the growing mode, because, as we have noted above, advection pushes charge into the bulging regions, so the repulsion becomes stronger in these regions leading to instability. On the other hand, the tangential stress

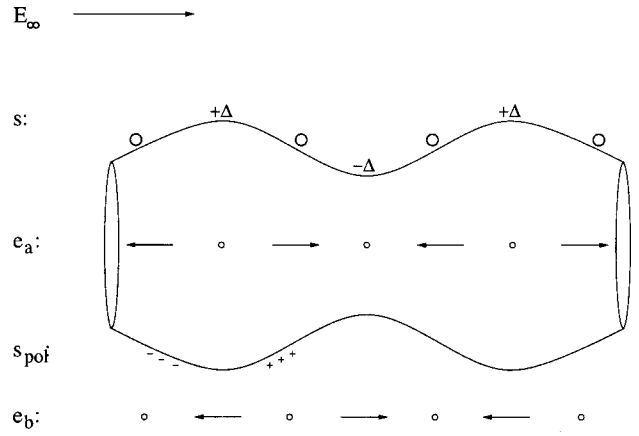

FIG. 9. Physical picture of an unstable perfect dielectric jet; the perturbation in surface charge density causes the electric field perturbation, e_a; the polarization charge (s_{pol}) tries to cancel out the penetration of the applied field, E_∞, and this causes the electric field perturbation, e_b.

stabilizes the jet by applying a line tension on the interface parallel to the flow. At long wavelengths, tangential stress stabilization beats charge self-repulsion; however, at small wavelengths (but still within the range of validity of this theory) the repulsion wins. These effects balance at the turnover wave number $k_c \sim 1/\sqrt{\beta}$. Figure 10 shows this competition.

2. Perfect conductors

Here the velocity response is the same as before, and the response of the two other fields is

$$\sigma_\epsilon = -\left(\sigma_0 + i\frac{\Omega_0}{2\pi\sqrt{\beta}\mathcal{L}k}\right)h_\epsilon, \tag{26}$$

$$e_\epsilon = -2\Omega_0 h_\epsilon. \tag{27}$$

In a perfectly conducting jet, charge flows (instantaneously) to the interface until the field normal to the interface is cancelled out. The electric field flux within the jet before perturbation is conserved throughout the instability, and the field lines simply get closer together in the narrowing regions and farther apart in the bulging regions. Thus, e_ϵ is π out of phase with h_ϵ (see Fig. 11).

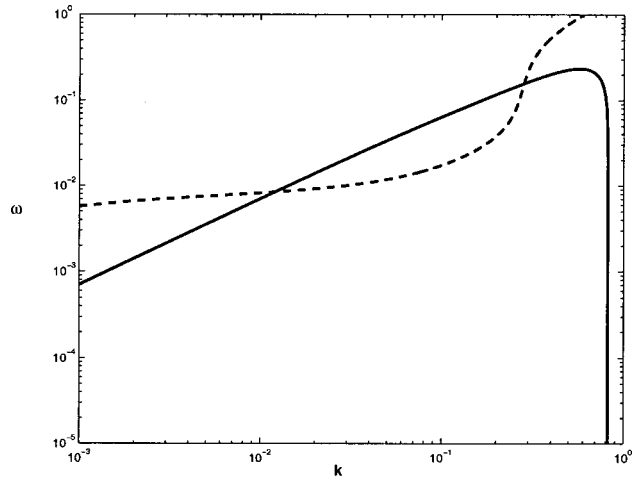

FIG. 10. For a perfect dielectric, the axisymmetric mode is destabilized by charge density (especially at high wave numbers). Comparison of the dispersion relation for a 0.1 cm diameter jet with $\nu = 1$ cm^2/s, $\epsilon = 78$, and $E_\infty = $ V/cm with no surface charge (solid line), and $\sigma_0 = 0.75$ (dashed line). The turnover at $k_c = \sqrt{6/\beta} \approx 0.27$ representing the competition between tangential stress stabilization and charge repulsion is evident.

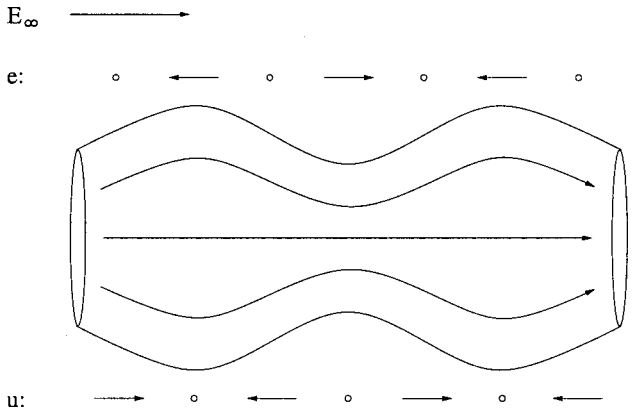

FIG. 11. Physical picture of an unstable perfectly conducting jet.

The charge density response is more complicated and is dictated by the requirement that there be no change in the electric flux within the jet. The term proportional to Ω_0, denoted e_a, excludes the penetration of applied field lines into the bulging fluid (see Fig. 12). This term is analogous to the term in the electric field response in the dielectric case that is proportional to Ω_0, except in that case it is the polarization that resists the field line penetration. The term e_b, proportional to σ_0, is negative, contrary to the case for perfect dielectrics. In order to counter the additional electric field within the jet due to a constant surface charge density on the perturbed interface, the charge density must decrease in the bulging regions and increase in the narrowing regions. Thus the repulsion becomes stronger in the narrowing regions and acts to stabilize the instability.

There are two terms that involve the background surface charge density. The first we have already discussed, and is just the suppression of the Rayleigh mode due to charge repulsion (Fig. 13). The second term involves a coupling between the externally applied field, Ω_0, and the surface charge density (the part that is proportional to σ_0). Because this term is imaginary, it always destabilizes the jet regardless of its sign. It also causes the frequency, ω, to be complex, so that the modes are oscillatory.

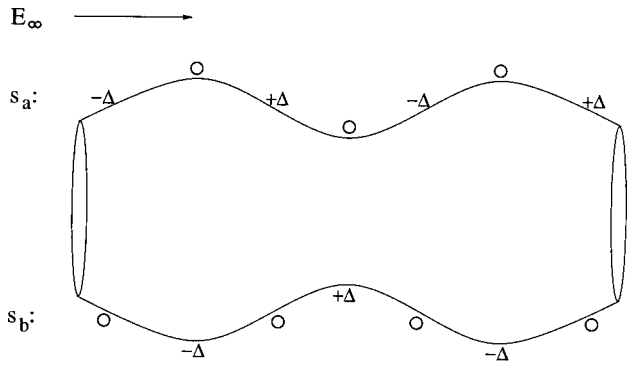

FIG. 12. Physical picture of an unstable perfectly conducting jet.

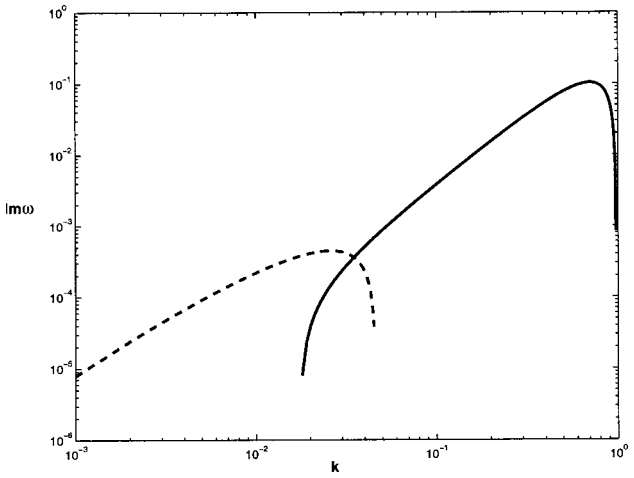

FIG. 13. For a perfect conductor, the axisymmetric mode is stabilized by charge density. Comparison of the dispersion relation for a 0.1 cm diam jet with $\nu=1$ cm^2/s, $\epsilon=78$ and $E_\infty=2/3$ kV/cm with no surface charge (solid line), and $\sigma_0=0.75$ (dashed line).

The response of the electric field to σ_0 is reflected in the formula for the growth rate of the mode given in formula (20). On one hand the Rayleigh mode is suppressed by the surface charge σ_0^2, while on the other the imaginary $\sigma_0\Omega_0$ term causes an unstable oscillatory instability. Hence, the existence of a static surface charge substantially modifies the ''Rayleigh mode'' we discussed above. The mode that reduces to the classical Rayleigh in the low Ω_0, σ_0 limit is always unstable even at very high fields. The transition represented by formula (21) does still exist, in that above this threshold field the mechanism for the instability is entirely electrical (and does not depend on the surface tension of the jet).

Finally, we consider the new modes that are due to finite conductivity. These modes are in general oscillatory. The reason follows from the leading order behavior for long wavelength oscillatory modes, which implies

$$\omega \approx (-1)^{1/3}(K^*\Omega_0^2)^{1/3}k^{2/3}, \tag{28}$$

where we have explicitly written $(-1)^{1/3}$ to remind the reader that there are three roots, two complex and one real. The two complex roots are oscillatory with positive growth rate. Formula (28) represents the balance between inertia and tangential electrical stress, $\rho\partial_t v \sim \sigma\Omega_0/r_0$, in the momentum balance equation, $\partial_t\sigma \sim 2K\Omega_0 r_0 h'$ in the charge advection equation, and $\partial_t h \sim -r_0 v'$ in the mass conservation equation. Hence, qualitatively the growing conducting mode arises from a phase lag between the free charge oscillation and the oscillation of the fluid.

D. Relation to previous work

The stability of a charged jet in an electric field has been previously considered by Mestel in two different limits: the ''weakly viscous limit''[36] in which the tangential stress on the jet is confined to a thin boundary layer near the surface of the jet, and the strongly viscous limit.[37] The weakly viscous limit occurs outside the regime of validity of the present theory, since we have assumed that tangential electrical stresses are much smaller than radial viscous stresses. However, it should be noted that this regime is also outside the regime of any experimental configuration that we are aware of. Mestel argues that this limit is relevant by noting that the Reynolds number $\mathrm{Re}_S=\sqrt{r_0\gamma/\rho\nu^2}$ is large for a thin jet of water, and hence there is a boundary layer near the surface of the jet. However, this Reynolds number (which compares the timescale for capillary contraction to the timescale for viscous diffusion across the jet radius) is irrelevant for the present problem; as has been emphasized above, tangential electrical stresses are much more important than capillarity. The correct ratio to consider whether a boundary layer can form near the surface of the jet is the ratio of the tangential stress to the radial viscous stress. For a mode of wavelength k, this ratio is (in dimensional units)

$$\frac{\sigma E/h}{\mu v/h^2} \sim \frac{KE_\infty^2 k r_0/\omega}{\mu/r_0^2\omega/k} \sim \frac{KE_\infty^2 r_0^3}{\mu}\frac{k^2}{\omega^2},$$

where we have used a typical surface charge density $\sigma \sim E_\infty r_0 k/\omega$ and a typical velocity $v\sim\omega/k$. Since $\omega\sim k^{2/3}$ at small k, this quantity is negligible as $k\to 0$, and hence in this limit, a boundary layer does not exist.

The strongly viscous limit[37] investigated by Mestel can in principle occur experimentally, and our results compare well with Mestel's. In the low k limit, both of us find that the growth rate obeys an equation of the form $a\omega^2+b\omega+c=0$. We both find the same limiting formula $a\to 3\tau$ (where τ is the conducting time defined above), and $b\to -1/2\tau(1+16\pi\sigma_0^2\log(k))$; we differ slightly in the formula for c (we find $c\to\Omega_0^2$ vs Mestel's $c\to\Omega_0^2(1+\sigma_0^2\tau)$).

III. ASYMPTOTIC THEORY OF A JET WITH A CURVED CENTERLINE

With these results in hand, we now turn towards an asymptotic theory for the bending modes of a jet, which are also important for experiments. We assume that the cross section of the jet remains circular, and we will ignore the coupling between the axisymmetric distortion of the jet and the bending of the centerline. This limits this theory's use to linear stability analysis. Nevertheless, we present the general method here, as the equations are readily generalized to the nonlinear case.

There are two pieces of intuition that need to be developed before we delve into the calculation itself. The first involves the calculation of the electric field of the jet. The reader will recall that when we derived the electric field equation for an axisymmetric jet, we expressed the potential outside the jet as if it were due to a linear monopole charge density spread along the jet's axis,

$$\overline{\phi}(\mathbf{x}) = \phi_\infty(\mathbf{x}) + \int dz' \frac{\lambda(z')}{|\mathbf{x}-\mathbf{x}'|},$$

where we have assumed that the capacitor plates that supply the electric field are far away from the region of interest. We will retain this assumption in the present analysis, for in experiments the region of nonaxisymmetric instability and breakup is always far removed from the boundaries of the system. The major difference from the previous (axisymmet-

ric) section is that when the jet bends the charge density along the jet is no longer uniform across the cross section of the jet, but in addition contains a *dipolar* component. (In general, if one were to develop an asymptotic theory for higher order nonaxisymmetric distortions of the jet, one would need to keep quadrapolar and higher terms in the charge density as well.) Hence, the equation for the electric potential will have the form,

$$\overline{\phi}(\mathbf{x}) = \phi_\infty(\mathbf{x}) + \int ds' \frac{\lambda(s')}{|\mathbf{x}-\mathbf{r}(s')|} + \int ds' \frac{\mathbf{P}(s')\cdot(\mathbf{x}-\mathbf{r}(s'))}{|\mathbf{x}-\mathbf{r}(s')|^3}, \tag{29}$$

where $\mathbf{P}$ is the linear dipole density along the centerline, and the centerline of the jet is located at $\mathbf{r}(s)$, parametrized by arc length. If the centerline is restricted to oscillations in a plane, then by symmetry the dipole density's direction must also be restricted to that plane.

The second piece of intuition is based on an idea of Mahadevan[43,44] concerning the dynamics of a bending fluid jet. We will consider only long wavelength modulations of the jet, so that the radius of curvature of the centerline, R, is much greater than the radius of the jet. In this limit, the equations of motion will then be structurally very similar to the equations for a slender, elastic rod under slight bending.[40] The equation of motion follows from considering both force balance and torque balance on the fiber, whose cross section is assumed to be both circular and constant in time.

To arrive at the form of the equations of motion, consider the force and torque balance on a small element of the jet of radius h and length ds. We will refer to the cylindrical portion of its surface as its tube, and to the circular ends as its caps. The centerline's tangent vector, $\hat{\mathbf{t}}$, normal to one cap is $\hat{\mathbf{t}}(s)$ and to the other $\hat{\mathbf{t}}(s+ds)$. Thus we allow for infinitesimal curvature of the centerline of this cross section.

Let $\mathbf{F}(s)$ be the resultant of the internal forces within the jet at s, and let $\mathbf{K}(s)$ be the resultant of all surface forces and external body forces per unit length. The equation for translational motion is then

$$\rho A \ddot{\mathbf{r}}(s) = \frac{\partial \mathbf{F}(s)}{\partial s} + \mathbf{K}, \tag{30}$$

where $A=\pi h^2$ is the cross-sectional area. The quantity, ρA, is the linear mass density, λ_m. If this were a simple string with constant tension, T, then $\mathbf{F}=T\hat{\mathbf{t}}$ and

$$\frac{\partial \mathbf{F}(s)}{\partial s} = \kappa T \hat{\mathbf{n}}, \tag{31}$$

where $\hat{\mathbf{n}}$ is the vector normal to the axis of the jet. If we restrict this string to move in the xz-plane, then $\kappa = X''(s)$ and we recover the familiar dispersion relation for waves on a string, $\omega/k=\sqrt{T/\lambda_m}$.

If the tangent vector varies slowly along the jet ($R \gg h$), then the jet is approximately in rotational equilibrium everywhere at every instant, and the equation for the rotational motion is then just torque balance (here we have neglected rotational accelerations since these are higher order terms),

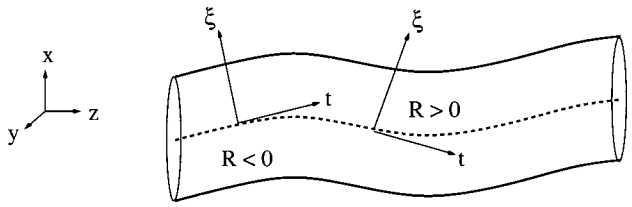

FIG. 14. Coordinates used in this calculation. The unit vector $\hat{\mathbf{y}}$ points out of the plane of the paper along the dashed centerline.

$$\frac{\partial(\mathbf{M}+\mathbf{N})}{\partial s} + \hat{\mathbf{t}}\times\mathbf{F} = 0, \tag{32}$$

where $\mathbf{M}$ ($\mathbf{N}$) is the moment of internal (external) stresses on the jet, and the reader will recognize the last term as the familiar $\boldsymbol{\tau}=\mathbf{r}\times\mathbf{F}$. In a perfect string $\mathbf{M}$ and $\mathbf{N}$ are zero, and $\mathbf{F}\propto\hat{\mathbf{t}}$. The idea of Mahadevan[43,44] is that in a fluid jet, viscous effects enter into the bending moment M, since this is where resistance to bending occurs. We will see below that in the present problem, the bending moment also includes a contribution from the polarization of the jet, due to the tendency of a polarized jet to align along the external field.

In writing this equation, we have assumed that there are no axisymmetric motions coupled to our bending jet, so that $h(s)$ is a constant. This implies inextensibility of the jet; because we are not allowed to stretch in the radial direction, to preserve volume we cannot stretch in an axial direction either. For this reason $\mathbf{F}$ should be viewed as a Lagrange multiplier associated with the inextensibility constraint. We also remark that if the cross section of the fiber is circular (as assumed), then the bending strain of the centerline is not coupled to twist (i.e., precession of the principal axes of inertia of the cross section of the jet), so this can be safely neglected.

To use these equations of motion, we must compute the torques and forces caused by the fluid and electrical stresses, a task to which we now turn.

A. Coordinate system

The coordinate system we will use is pictured in Fig. 14. We form an orthogonal, right-handed coordinate system $\hat{\mathbf{x}}$, $\hat{\mathbf{y}}$, and $\hat{\mathbf{z}}$, such that $\hat{\mathbf{z}}$ points in the direction of the unperturbed flow. We will allow the jet's centerline to deform in the xz-plane (ignoring effects related to the torsion of the centerline). Define $\hat{\mathbf{t}}$ to be the tangent vector to the jet's centerline, and $\hat{\boldsymbol{\xi}}$ to be a vector normal to the centerline that, for an unperturbed jet, points in the same direction as $\hat{\mathbf{x}}$. (Note that this is slightly unconventional; the normal vector to a sinusoidal curve usually flips direction; so that $\hat{\boldsymbol{\xi}}$ is well-defined at all points on the curve, we will bury the change of sign in our definition of the curvature of the centerline.) The binormal always points in the direction of $\hat{\mathbf{y}}$, so we retain that notation. We define the curvature such that, in this coordinate system,

$$\frac{\partial \hat{\mathbf{t}}}{\partial s} = \kappa_{\text{jet}} \hat{\boldsymbol{\xi}} = \frac{1}{R} \hat{\boldsymbol{\xi}},$$

$$\frac{\partial \hat{\boldsymbol{\xi}}}{\partial s} = -\kappa_{\text{jet}} \hat{\mathbf{t}} = -\frac{1}{R} \hat{\mathbf{t}},$$

where ∂_s is the derivative with respect to arc length of the centerline. The angle θ will be the angle measured in the ξy-plane from the ξ-axis in a counterclockwise direction with respect to $\hat{\mathbf{t}}$.

The oscillation of the centerline will be parametrized by a function $X(z,t)$, so that its locus is described in Cartesian coordinates by

$$\mathbf{r}(z,t) = z\hat{\mathbf{z}} + X(z,t)\hat{\mathbf{x}}. \tag{33}$$

We can then calculate the tangent and normal vectors and the curvature,

$$\hat{\mathbf{t}}(z,t) = \frac{1}{\sqrt{1+X'^2}}[\hat{\mathbf{z}} + X'(z,t)\hat{\mathbf{x}}] \tag{34}$$

$$\approx \hat{\mathbf{z}} + X'\hat{\mathbf{x}}, \tag{35}$$

$$\hat{\boldsymbol{\xi}}(z,t) = \frac{1}{\sqrt{1+X'^2}}[-X'(z,t)\hat{\mathbf{z}} + \hat{\mathbf{x}}] \tag{36}$$

$$\approx -X'\hat{\mathbf{z}} + \hat{\mathbf{x}}, \tag{37}$$

$$\kappa_{\text{jet}}(z,t) = \frac{1}{R} = \frac{X''}{1+X'^2} \approx X''. \tag{38}$$

In general we will assume that the jet is only slightly curved, that is, that the radius of curvature of the centerline, R, is much larger than the radius of the jet, h, which is equivalent to $\kappa_{\text{jet}} \ll 1/h$. As previously mentioned, we constrain the jet cross section to remain a circle with a constant radius, h.

We can write down the mapping, which is not one-to-one, from local (ξ,y,s) coordinates to Cartesian (x,y,z) coordinates. To determine this mapping, we first compute s in terms of z along the centerline (call this s_0),

$$s_0(z) = \int_0^z dz' \sqrt{1+X'^2}.$$

This function has an inverse, $z_0(s)$, which is the z-coordinate of a point on the centerline at arclength s. We can then compute the desired mapping by following $\mathbf{r}$ along the curve to $z_0(s)$, then following the normal vectors $\hat{\boldsymbol{\xi}}$ and $\hat{\mathbf{y}}$ by the proper amount,

$$(\xi,y,s) = \mathbf{r}(z_0(s)) + y\hat{\mathbf{y}} + \xi\hat{\boldsymbol{\xi}}$$

$$= z_0(s)\hat{\mathbf{z}} + X\hat{\mathbf{x}} + y\hat{\mathbf{y}} + \frac{\xi}{\sqrt{1+X'^2}}(-X'\hat{\mathbf{z}} + \hat{\mathbf{x}})$$

$$= \hat{\mathbf{z}}\left(z_0(s) - \frac{\xi X'}{\sqrt{1+X'^2}}\right) + y\hat{\mathbf{y}} + \hat{\mathbf{x}}\left(X + \frac{\xi}{\sqrt{1+X'^2}}\right),$$

where X is understood everywhere to be evaluated at $z_0(s)$ and t. For small curvatures, this is approximately equal to

$$(\xi,y,s) \approx \hat{\mathbf{z}}(z - \xi X') + y\hat{\mathbf{y}} + \hat{\mathbf{x}}(X + \xi), \tag{39}$$

where X is evaluated at z and t.

B. Electric field equation

We now need to derive an asymptotic approximation to the integral Eq. (29) for the electric field. The derivation will proceed in much the same way as the axisymmetric derivation: after approximating the integrals, we will express both the effective charge density λ and the dipole density P in terms of the free charge density and the electric field itself using Gauss's Law. Putting everything together will give an equation for the field. For the present purposes it is only necessary to carry out this derivation to lowest order in the distortion of the centerline from straight.

The dipole density P is caused by the distortion of the centerline of the jet. This implies that (a) $\mathbf{P}(s)$ points in the ξ direction, and (b) the variation in $\mathbf{P}(s)$ occurs on the length scale of the modulation of the jet. It then follows that (to lowest order in the distortion of the centerline)

$$\int ds' \frac{\mathbf{P}(s')\cdot(\mathbf{x}-\mathbf{x}(s'))}{|\mathbf{x}-\mathbf{x}(s')|^3} \approx xP(z)\int dz' \frac{1}{((z'-z)^2+r^2)^{3/2}}$$

$$\approx \frac{xP(s)}{r^2}, \tag{40}$$

where at this order $s \approx z$ and $\hat{\boldsymbol{\xi}} \approx \hat{\mathbf{x}}$.

There is also a correction to the potential from the curvature of the centerline. If the local radius of curvature of the jet is R, then

$$|\mathbf{x}(s) - \mathbf{x}(s')| = |\xi\hat{\boldsymbol{\xi}} + y\hat{\mathbf{y}} - \mathbf{x}(s')|$$

$$\approx \left[s'^2\left(1 - \frac{\xi}{R}\right) + \xi^2 + y^2\right]^{1/2}. \tag{41}$$

Thus,

$$\int ds' \frac{\lambda(s')}{|\mathbf{x}-\mathbf{x}(s')|} = \int ds' \frac{\lambda(s')}{\left(s'^2\left(1-\frac{\xi}{R}\right)+r^2\right)^{1/2}}$$

$$\approx 2\lambda(s)\ln\frac{L}{r} + \frac{\xi\lambda(s)}{R}\ln\frac{L}{r}, \tag{42}$$

where L is the characteristic axial length scale (determined in practice by the shape of a jet as it thins away from the nozzle). The leading order term is familiar from the axisymmetric calculation, and in addition there is a nonaxisymmetric correction due to the curvature of the centerline. Putting it together, we now have that

$$\overline{\phi}(\xi,y,s) = \phi_\infty + 2\lambda(s)\ln\frac{L}{r} + \frac{\xi\lambda(s)}{R}\ln\frac{L}{R} + \frac{\xi P(s)}{r^2}, \tag{43}$$

where ξ is the coordinate in the principal normal direction, and s is the arc length.

With this equation for the field outside the jet, we can compute the equation for the field inside the jet by demanding that the electrical boundary conditions at the interface are satisfied, namely that the tangential component of the field is continuous across the interface and the jump in the normal $\epsilon\mathbf{E}$ is given by the free surface charge. The electric field inside the jet is the sum of a piece directed along the principal normal, i.e., along the direction of polarization, and a

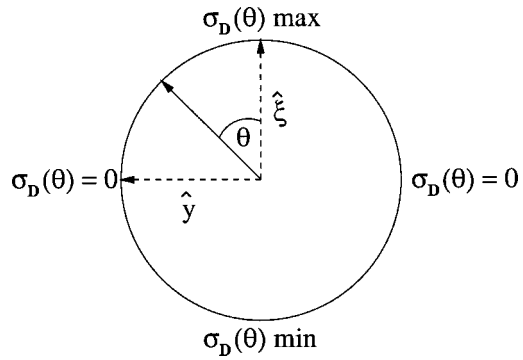

FIG. 15. Picture of the cross section of a jet. $\hat{\mathbf{t}}$ points out of the plane of the page. The asymmetric part of the surface charge density, $\sigma_D(\theta) = \sigma_D \cos\theta$, is shown for $\sigma_D > 0$.

piece directed along the tangent to the centerline, which we denote by

$$\mathbf{E} = E_1 \hat{\boldsymbol{\xi}} + E_t \hat{\mathbf{t}}. \tag{44}$$

The free charge density is composed of both a monopole and a dipole contribution $\sigma = \sigma_0(s) + \sigma_D(s)\cos\theta$, where θ is the angular coordinate around a given cross section of the jet (see Fig. 15). Applying the boundary conditions yields, after some algebra,

$$E_t = \overline{E_t} = -\partial_s \overline{\phi} = \mathbf{E}_\infty \cdot \hat{\mathbf{t}} - 2\ln\left(\frac{1}{\chi}\right)\lambda'(s) - \ln\left(\frac{1}{\chi}\right)\frac{h(s)\lambda'(s)\cos\theta}{R} - \frac{P'(s)\cos\theta}{h(s)}, \tag{45}$$

$$E_1 = \mathbf{E}_\infty \cdot \hat{\boldsymbol{\xi}} - \ln\left(\frac{1}{\chi}\right)\frac{\lambda}{R} - \frac{P}{h^2} = \frac{2}{\beta+2}\left(\mathbf{E}_\infty \cdot \hat{\boldsymbol{\xi}} - \frac{2\pi\sigma_D}{\overline{\epsilon}}\right) - \frac{2}{(\beta+2)}\frac{\lambda}{R}\ln\left(\frac{1}{\chi}\right), \tag{46}$$

and

$$P = \frac{\beta}{2}h^2 E_1 + \frac{\pi}{2\overline{\epsilon}}h^2\sigma_D. \tag{47}$$

There is also a correction to the equivalent line charge density λ from the curvature of the centerline. From the axisymmetric calculation, we know

$$\lambda(s) = -\frac{\beta}{4}\partial_s(h^2 E_t)' + \frac{2\pi h\sigma}{\overline{\epsilon}}. \tag{48}$$

If we assume that h is constant and that E_t is given by the axisymmetric (θ independent) part of Eq. (45), then we have

$$\lambda(s) = -\frac{\beta}{4}h^2\partial_s E_t + \frac{2\pi h\sigma_0}{\overline{\epsilon}} = -\frac{\beta}{4}h^2\partial_s\left(\mathbf{E}_\infty \cdot \hat{\mathbf{t}} - 2\ln\left(\frac{1}{\chi}\right)\lambda'(s)\right) + \frac{2\pi h\sigma_0}{\overline{\epsilon}} = \frac{\beta}{4}h^2\left(-\frac{1}{R}\mathbf{E}_\infty \cdot \boldsymbol{\xi} + 2\ln\left(\frac{1}{\chi}\right)\lambda''(s)\right) + \frac{2\pi h\sigma_0}{\overline{\epsilon}}. \tag{49}$$

Hence, in the absence of free charge, λ is of order $1/R^2$. Furthermore, λ' is of order $1/R^3$ even with surface charge, since σ_0 is assumed constant in this derivation. Thus, if we are only interested in leading order terms in the centerline curvature, we can rewrite E_1 as

$$E_1 = \frac{2}{\beta+2}\left(\left[\mathbf{E}_\infty \cdot \hat{\boldsymbol{\xi}} - \frac{2\pi}{\overline{\epsilon}}\sigma_D\right] - 2\pi\frac{h}{R}\sigma_0\ln\left(\frac{1}{\chi}\right)\right) \tag{50}$$

and P as

$$P = \frac{\beta h^2}{(\beta+2)}\mathbf{E}_\infty \cdot \hat{\boldsymbol{\xi}} + \frac{4\pi h^2}{\overline{\epsilon}(\beta+2)}\left(\sigma_D - \frac{\beta}{2}\frac{h\sigma_0}{R}\ln\left(\frac{1}{\chi}\right)\right). \tag{51}$$

Physically, the field E_1 perpendicular to the centerline of the jet is caused by the fact that the dipolar charge distribution does not completely cancel out the applied field inside the jet (terms in parentheses), and a "fringe" field results from curving the line charge λ. For a perfect conductor with $\sigma_0 = 0$ the cancellation of E_1 inside the jet leads to a simple relation between the dipolar density and the field, $2\pi\sigma_D/\overline{\epsilon} = \mathbf{E}_\infty \cdot \hat{\boldsymbol{\xi}}$.

C. Forces and torques

Now that we understand the electrostatics, we can proceed with calculating the electrical stresses to get the equations of motion of the centerline. We need to compute the moments (**M**), torques (**N**), and forces (**K**) on the jet. The internal moments are obtained by integrating the torque produced by the tangent–tangent component of the stress tensor,

$$T_{tt} = -p + 2\mu\hat{\mathbf{t}}\cdot((\hat{\mathbf{t}}\cdot\boldsymbol{\nabla})\mathbf{u}) + \frac{\epsilon}{8\pi}(E_t^2 - E_\xi^2 - E_y^2) \tag{52}$$

over a cross section, S. The moment

$$M_\xi = \int\int_S T_{tt} y\, dA \tag{53}$$

$$= 0 \tag{54}$$

vanishes, since the stress tensor is even in y. The other moment, however, is nonzero. There are two contributions to this moment, arising from electrical and viscous forces. After some straightforward algebra, the electrical moment is

$$M_y^E = -\int\int_S T_{tt}^E \xi\, dA \tag{55}$$

$$= \frac{\epsilon}{16}P' h^2 E_{\infty_t}. \tag{56}$$

This moment arises from the fact that a polarized jet will try to align with the applied electric field.

A moment also arises from the viscous response of the fluid.[43,44] Intuitively, in an elastic fiber, elastic forces resist the bending of the jet, and this resistance gives rise to a classical elastic bending moment,[40] which is just the curvature of the fiber multiplied by its bending modulus. Viscosity

plays an analogous role in a bent viscous jet; however instead of the moment being proportional to the curvature, it turns out to be proportional to the time derivative of the curvature.[43] The reason for this is that the viscous stress is proportional to the *rate* of strain, whereas in a solid the elastic stress is proportional to the strain. Thus we anticipate that $M_y^F \propto \mu \dot{k}_{\text{jet}}$ (and M^F is the fluid component of the moment). For this formula to be dimensionally correct, we must multiply it by h^4, yielding

$$M_y^F = -A\mu h^4 \dot{\kappa}_{\text{jet}}, \tag{57}$$

where the sign reflects the fact that viscosity resists bending, and the coefficient A must be calculated. It turns out that $A = -3/4\pi$.[34]

The external torque **N** from surface forces is simpler to derive and involves only electrostatic effects. By symmetry $N_\xi = 0$, so we must only compute N_y. In order to do this, we integrate $\mathbf{r}\times\mathbf{F}$ across the boundary (denoted by brackets) of the jet, where **F** is the external surface stress. Straightforward algebra yields

$$\begin{aligned} N_y &= -\int_C dC ds(\theta)\xi \langle \hat{n}_i T_{ij}^E \hat{t}_j \rangle \\ &\approx ds\,\pi h^2 \left[\frac{E_{\infty_t}\sigma_0 h}{R} + \frac{P'\sigma_0}{h} - E_{\infty_t}\sigma_D \right]. \end{aligned} \tag{58}$$

This moment is entirely caused by the electrical tangential stress σE_t. The first two terms are the moment due to the stress on the axisymmetric part of the charge density, which produces a moment because the jet is curved. The third term is the moment due to the tangential stress on the asymmetric portion of the charge density, on which the field pushes on one side of the jet and pulls on the other side.

Finally we compute the external forces **K** on the jet. Note that internal forces (e.g., from viscosity) are absorbed in the tension **F**. There are two external forces, surface tension and an electrical force.

The surface tension force arises because when the jet is bent, a segment of rest length *ds* has more surface area farther from the center of curvature of the jet. The surface tension force is therefore larger farther from the center of curvature, which tends to reduce the bending of the jet. A calculation gives the net force

$$\begin{aligned} \mathbf{K}^F &= -\gamma \int_0^{2\pi} d\theta \left(1 - \frac{h\cos\theta}{R} \right) (\hat{\boldsymbol{\xi}}\cos\theta + \hat{\mathbf{y}}\sin\theta) \\ &= \hat{\boldsymbol{\xi}}\gamma \frac{\pi h^2}{R}. \end{aligned} \tag{59}$$

The electrical force follows from integrating the unbalanced electrical force over the interface. After some algebra, this gives

$$\begin{aligned} K_j^E &= \frac{1}{ds}\int dC ds(C) \left\langle \frac{\epsilon}{8\pi} ((E_n^2 - E_t^2 - E_\theta^2)\hat{n}_j + 2E_n(E_t \hat{t}_j \right. \\ &\quad \left. + E_\theta \hat{\theta}_j)) \right\rangle \\ &= \pi h \hat{\boldsymbol{\xi}} \left[-\frac{4\pi}{\overline{\epsilon}} \frac{h\sigma_0^2}{R} \ln\left(\frac{1}{\chi}\right) + 2E_{\infty_\xi}\sigma_0 - \frac{\overline{\epsilon}}{4\pi} \frac{E_\infty P'(s)}{h} \right]. \end{aligned} \tag{60}$$

Putting everything together, we obtain

$$\begin{aligned} \mathbf{K} &= \mathbf{K}^E + \mathbf{K}^F \\ &= \pi h \hat{\boldsymbol{\xi}} \left[-\frac{4\pi\sigma_0^2 h}{R\overline{\epsilon}} \ln\left(\frac{1}{\chi}\right) + \frac{\gamma}{R} + 2E_{\infty_\xi}\sigma_0 - \frac{\overline{\epsilon}\beta}{4\pi} \frac{E_\infty P'}{h} \right]. \end{aligned} \tag{61}$$

The first two terms represent line tensions (or compressions) that are nonzero only when the jet is curved. Surface tension pulls on the ends of our piece of jet, so it stabilizes the jet against curvature. The self-repulsion of charge, on the other hand, pushes on the ends of the jet, so it is destabilizing. The third term is the force of the applied electric field normal to the jet on the axisymmetric surface charge density (again, only possible for curved jets). The final term is the force due to the nonaxisymmetric portion of the electrostatic pressure, $E^2/8\pi$. This term tries to align the surface of the jet with the curved local field lines.

Combining these results gives the equation for the motion of the centerline. From torque balance we obtain the tension in the fiber to be

$$\begin{aligned} F_x &= -\partial_s M_y - \partial_s N_y \\ &= \partial_s \left[-\frac{3\pi}{4}\mu h^4 \dot{\kappa}_{\text{jet}} - \frac{\epsilon}{16} P' h^2 E_{\infty_t} \right] \\ &\quad + \pi h^2 \left[\frac{E_{\infty_t}\sigma_0 h}{R} + \frac{P'\sigma_0}{h} - E_{\infty_t}\sigma_D \right]. \end{aligned} \tag{62}$$

Using this in the force balance equation gives our final result

$$\begin{aligned} \rho\pi h^2 \ddot{X}(s) &= \partial_{ss}\left[-\frac{3\pi}{4}\mu h^4 \dot{\kappa}_{\text{jet}} - \frac{\epsilon}{16} P' h^2 E_{\infty_t} \right] \\ &\quad + \pi h^2 \partial_s \left[\frac{E_{\infty_t}\sigma_0 h}{R} + \frac{P'\sigma_0}{h} - E_{\infty_t}\sigma_D \right] \\ &\quad - \frac{\overline{\epsilon}\beta P' E_\infty}{4} + \frac{\pi h\gamma}{R} - \frac{4\pi^2 h^2 \sigma_0^2}{\overline{\epsilon} R} \ln\left(\frac{1}{\chi}\right) \\ &\quad + 2\pi h E_{\infty_\xi}\sigma_0. \end{aligned} \tag{63}$$

We now nondimensionalize according to the usual scheme, with h scaled by r_0,

$$\ddot{X}(s)=\partial_{ss}\left[-\frac{3}{4}\nu^*\dot{\kappa}_{\rm jet}-\frac{\overline{\epsilon}(\beta+1)}{16\pi\sqrt{\beta}}\Omega_{0_t}P'\right]+\beta^{-(1/2)}\partial_s\left[\frac{\Omega_{0_t}\sigma_0}{R}+\overline{\epsilon}\sigma_0P'-\Omega_{0_t}\sigma_D\right]-\frac{\overline{\epsilon}\sqrt{\beta}\Omega_{0_t}}{4\pi}P'+\frac{1}{R}-\frac{4\pi\sigma_0^2}{R}\ln\left(\frac{1}{\chi}\right)+2\beta^{-(1/2)}\sigma_0\Omega_{0_\xi}. \tag{64}$$

D. Conservation of charge

To close the problem, we still need an equation for σ_D. This equation comes from the general charge conservation equation for a stripe of charge of width $hd\theta$ and length ds at an angle θ from the principal normal, $\hat{\boldsymbol{\xi}}$,

$$\partial_t(hd\theta\sigma)+\partial_s(v(s,\theta)hd\theta\sigma)=hd\theta\cos\theta KE_1. \tag{65}$$

Neglecting the advection velocity, after some algebra we obtain

$$\partial_t\sigma_D=K\left(\frac{2}{\beta+2}\mathbf{E}_\infty\cdot\hat{\boldsymbol{\xi}}-\frac{4\pi}{\overline{\epsilon}(\beta+2)}\left(\sigma_D+\frac{h}{R}\sigma_0\right)\right). \tag{66}$$

We can nondimensionalize this to obtain

$$\partial_t\sigma_D=K^*\left(\frac{2}{\beta+2}\Omega_{0_\xi}-\frac{4\pi\sqrt{\beta}}{\beta+2}\left(\sigma_D+\frac{h}{R}\sigma_0\right)\right). \tag{67}$$

The two terms on the left-hand side are the convective derivative of the ''dipole'' charge density, σ_D. The right-hand side is the conduction current density due to the nonaxisymmetric field within the jet.

E. Linear stability

It is now a simple matter to calculate the dispersion relation for nonaxisymmetric modes. We describe the centerline in nondimensional coordinates by $\mathbf{r}(z,t)=z\hat{\mathbf{z}}+\varepsilon e^{\omega t+ikz}\hat{\mathbf{x}}$, and σ_D by $\sigma_D(z,t)=CX(z,t)$, where C can in general be complex. After much algebra we arrive at the dispersion relation

$$\omega^2=-\frac{3}{4}\nu^*\omega k^4-4\pi\sigma_0^2k^2\ln(k)-ik\frac{2\sigma_0\Omega_0}{\sqrt{\beta}}-\frac{ik\Omega_0}{\sqrt{\beta}}(\sigma_0k^2+C)-k^2+\left(\Omega_0\left[-\frac{1}{4\pi}+\frac{(\beta+1)k^2}{16\pi\beta}\right]+\frac{ik\sigma_0}{\beta}\right)\times\frac{\sqrt{\beta}}{\beta+2}[k^2\sqrt{\beta}\Omega_0+ik(4\pi C+2\pi\beta\sigma_0k^20)], \tag{68}$$

with C given by

$$C=-\frac{ik\dfrac{2K^*\Omega_0}{\beta+2}+\dfrac{4\pi\sqrt{\beta}K^*}{\beta+2}\sigma_0k^2}{\dfrac{4\pi\sqrt{\beta}K^*}{\beta+2}+\omega}. \tag{69}$$

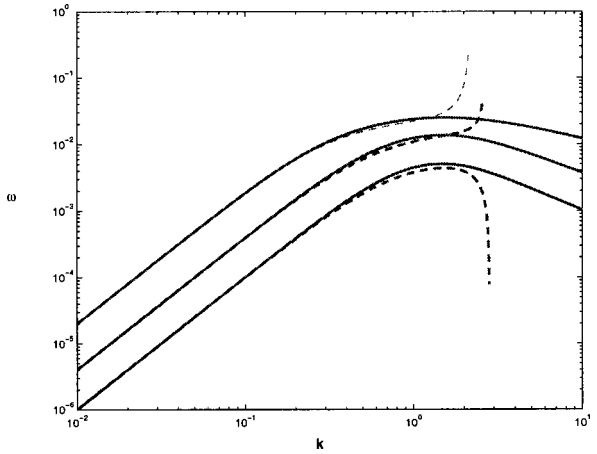

FIG. 16. Comparison of our inviscid whipping mode formula (dashed) with Saville's exact formula (solid) for $K^*=0.7$ and for field strengths $\Omega_0=2.2,4.4,9.8$. (The maximum growth rate increases with the field strength.) Our asymptotic formula deviates from Saville's when $k\approx1$, because the approximations underlying it break down.

1. Electric field without surface charge

We pause at this stage to study the dynamics when there is an external electric field but no surface charge. We first compare our formula to Saville's formula[33] for inviscid jets without surface charge. We set C and σ_0 to zero, and obtain

$$\omega^2=A\nu^*\omega k^4-k^2-\left(\frac{1}{4\pi}-\frac{(\beta+1)k^2}{8\pi\beta}\right)\frac{\beta\Omega_0^2}{\beta+2}k^2. \tag{70}$$

In the limit of vanishing fluid viscosity this is

$$-\omega^2=k^2+\frac{\beta}{4\pi}\frac{\Omega_0^2k^2}{\beta+2}-\frac{(\beta+1)}{8\pi(\beta+2)}\Omega_0^2k^4. \tag{71}$$

This is precisely the same as the long wavelength limit of Saville's[33] formula for perfect dielectrics.

We can also compare this formula for perfect conductors, i.e., in the infinitely conducting limit. In this limit, the normal field is completely cancelled out inside the jet (i.e., $E_1=0$) so

$$C=-i\frac{\Omega_0k}{2\pi\sqrt{\beta}}. \tag{72}$$

This implies that without surface charge we have

$$-\omega^2=k^2+\frac{\beta+2}{4\pi\beta}\Omega_0^2k^2-\frac{\beta+2}{16\pi\beta}\Omega_0^2k^4,$$

so there is no instability. This formula exactly agrees with Saville's result[33] in the long wavelength limit. For both perfect dielectrics and perfect conductors, the electrical properties actually enhance the stabilization of the jet over the effect of surface tension acting alone; this is analogous to the axisymmetric instability described in the previous section.

It should be remarked that these dispersion relations for both dielectric jets and perfectly conducting jets show that the fiber responds exactly like a string under tension. The velocity for waves on a perfectly conducting jet is

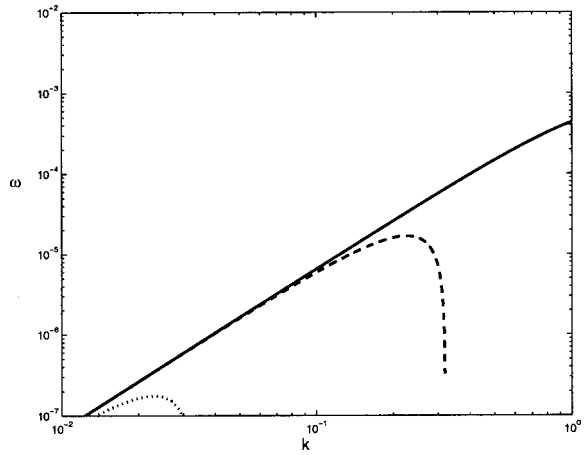

FIG. 17. The dependence of the growth rate on viscosity for $E_\infty = 1$ kV/cm, $K = 0.01$ μS/cm, $\beta = 80$, $r_0 = 0.05$ cm, and $\gamma/\rho = 73$. The uppermost solid curve shows the dispersion relation for an inviscid fluid, the middle curve has $\mu = 0.01$ P, and the lowermost curve has $\mu = 1$ P. Even a very small viscosity shifts the most unstable wavelength into the $k<1$ long wavelength regime, and greatly suppresses the growth rate.

$$c^2 = \left(\frac{\gamma}{\rho r_0} + \frac{(\beta+2)E_\infty^2}{4\pi} \right). \tag{73}$$

When the electrical conductivity is finite, the whipping of the jet becomes unstable; as in the case of the axisymmetic modes, the instability is caused by an imbalance in the tangential stress on the interface, caused by the interaction of the induced surface charge density and the tangential electric field.

Figure 16 compares our predicted dispersion relation in the low viscosity limit, with Saville's corresponding formulas. As expected, the formulas agree at low wave numbers; the long wavelength theory deviates from the exact formulas when $k>1$.

The reader may at this point be disturbed by the fact that Fig. 16 predicts a short wavelength instability, which—if true experimentally—would invalidate the long wavelength assumption underlying this entire analysis. Indeed, Saville's analysis predicts that for a jet of water the wavelength of the instability is much smaller than the wavelength of the fiber. However, we remind the reader that (a) Saville disregarded both viscosity and surface charge in his plotted growth rates;[33] and (b) experiments[29] show demonstrably in all cases reported that the instability is long wavelength relative to the radius of the jet.

Figure 17 shows the influence of viscosity on a finite conductivity jet without surface charge. Even a very small viscosity shifts the most unstable wave number into the $k<1$ long wavelength regime; also, a tenfold increase in the viscosity decreases the growth rate by a factor of 10. This demonstrates that the prediction of a short wavelength instability is corrected when viscosity is included. The attentive reader will at this point, note, however, the existence of another problem, namely, the growth rate for the whipping mode for water is so suppressed that now the axisymmetric mode is predicted to go unstable before the whipping mode, contradicting experiments.

The physical mechanisms behind these results can be uncovered by rewriting the dispersion relation in the limit of very large (but not infinite conductivity). We neglect surface charge, and will work in dimensionful units in this subsection to more clearly expose the mechanisms. We first rewrite Eq. (67) as

$$\sigma_D = \frac{\overline{\epsilon}\mathbf{E}_\infty \cdot \hat{\boldsymbol{\xi}}}{2\pi} - \frac{\overline{\epsilon}\beta+2}{4\pi K}\dot{\sigma}_D, \tag{74}$$

and then iteratively solve for σ_D to leading order in K^{-1}. This gives (to leading order)

$$\sigma_D = \frac{\overline{\epsilon}\mathbf{E}_\infty \cdot \hat{\boldsymbol{\xi}}}{2\pi} - \frac{\overline{\epsilon}(\beta+2)}{8\pi^2}\frac{\overline{\epsilon}}{K}\partial_t(\mathbf{E}_\infty \cdot \hat{\boldsymbol{\xi}}). \tag{75}$$

Using this approximation we can evaluate the forces and torques that act on the jet in the high conductivity limit, to expose the basic mechanisms. The acceleration of the centerline can be expanded in the form,

$$\rho h^2 \pi \ddot{X} = A_1 \frac{1}{R} + A_2 \partial_t \frac{1}{R} - A_3 \partial_t \partial_{ss} \frac{1}{R}, \tag{76}$$

where the A_i are given below. If the signs of the A_i are positive (as defined above) then each of the terms listed above are stabilizing. The term A_1 corresponds to a tension, and results in a wave-like response. The terms A_2 and A_3 correspond to damping of this wave. The form of these coefficients in the limit of high conductivity and zero net surface charge density is

$$A_1 = \pi h \gamma + \frac{h^2 E_\infty^2 (\beta+2)}{4}, \tag{77}$$

$$A_2 = -\frac{E_\infty^2 \overline{\epsilon}(\beta+1)}{4\pi}\frac{\overline{\epsilon}}{K}h^2, \tag{78}$$

$$A_3 = \frac{3}{4}\pi\mu h^4 + \frac{\overline{\epsilon}}{32\pi}h^4 E_\infty^2 \frac{\overline{\epsilon}}{K}. \tag{79}$$

The tension A_1 is the same form as for a perfect conductor, and represents the enhancement of the tension in the jet due to the applied electric field. The leading order effect of finite conductivity is given by A_2 and the second term in A_3. The A_2 term is *destabilizing* and is the reason for the finite conductivity instability shown in Fig. 16. This instability can be traced back to the external torque $\mathbf{N}$ on the jet due to the tangential electric stress. This instability is stabilized by the two physical effects contained in A_3; these correspond to the viscous moment, and (part of the) the electrical moment. When the viscous part dominates the maximum growth rate of the instability,

$$\omega_{\max} \sim h^2 E_\infty^2 (\mu K)^{-1}.$$

This explains the trends shown in Fig. 17. Also note that at fixed field strength, the growth rate of the instability decays with increasing conductivity, while the wave number remains the same.

When the viscous moment is smaller than the electrical moment (cf. the two terms in $A_3, \mu < \overline{\epsilon}^2 E_\infty^2/(24K\pi^2)$) the maximum growth rate occurs when $k>1$, outside the range

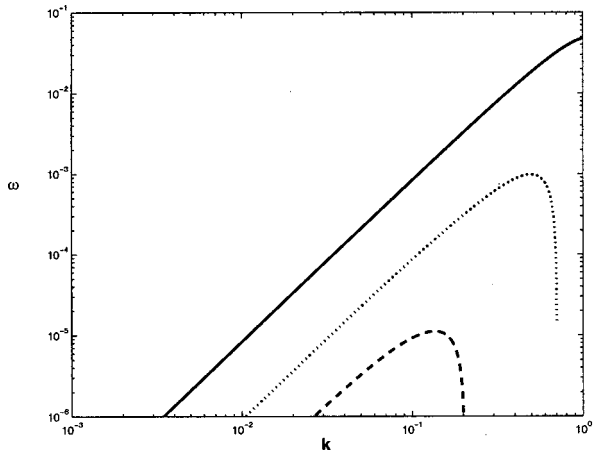

FIG. 18. The dependence of the growth rate on surface charge for a $r_0=100$ μm water jet ($K=0.01$ μS/cm, $\beta=80$, $\nu=0.01$) in an electric field $E_\infty=1$ kV/cm. The lowermost solid curve shows the dispersion relation for an uncharged fluid, the middle curve has $\sigma_0=0.01$ and the solid curve has $\sigma_0=0.1$.

of the long wavelength theory. For a high field of 10 kV/cm with a modest conductivity 1 μS/cm, the critical viscosity $10^{-3}\,\mathrm{cm}^2/\mathrm{s}$. Hence even water is sufficiently viscous to damp the instability! This is the essential reason why our results differ so markedly from Saville's analysis in the limit of vanishing viscosity. When viscosity does not damp the instability, there is a breakdown of the long wavelength theory, because the instability is peaked at high k. This represents a real physical effect: the jet will try to bend on a wavelength smaller than its radius, which could correspond to forming a kink. Note that for fixed fluid viscosity, there is a critical electric field depending on viscosity and conductivity above which this will occur.

2. Surface charge

We will now study the effect of surface charge on the jet stability. First, we remark that our formulas reduce to those found previously for perfectly conducting charged cylinders in no external electric field. For example, in the limit of high viscosity, our formula reduces to

$$\omega=-\frac{4}{3\nu^*}\frac{1}{k^2}(1+4\pi\sigma_0^2\log k) \tag{80}$$

as found previously by Saville and Huebner.[34,35] Surface charge destabilizes the jet at small wave numbers, due to plain old charge repulsion. The divergence represented in this formula as $k\to 0$ is unphysical and reflects the fact that this balance is asymptotically inconsistent; at long wavelengths, inertia is always important. For small surface charge densities, the jet is a string with a tension (in dimensional units)

$$\pi\gamma h+\frac{4\pi^2h^2\sigma_0^2}{\bar{\epsilon}}\log(k).$$

When the surface charge density beats surface tension this results in an instability.

Figure 18 shows the effect of surface charge on the axisymmetric instability for a 100 μm water jet ($\beta=80$, $\nu=0.01$, $K=0.01$ μS) in a 1 kV/cm external field. Upon increasing the dimensionless surface charge from 0 to 0.1, the most unstable wave number increases from $k\approx 0.1$ to $k=0.8$, and moreover the growth rate of the instability increases by about four orders of magnitude!

To develop a physical understanding of this result, we follow the same procedure as above for the electrical case: The equation for the force now takes the form (to leading order),

$$\rho\pi h^2\ddot{X}=(A_1+B_1)\frac{1}{R}+B_2\partial_2\frac{1}{R}+B_3\partial_{ss}\frac{1}{R}+A_2\partial_t\frac{1}{R}$$

$$-(A_3+B_4)\partial_{ss}\partial_t\frac{1}{R}+2\pi h\sigma_0\,\mathbf{E}_\infty\cdot\xi, \tag{81}$$

where the A_i are the electrical coefficients, and the B_i are the modifications due to surface charge. Note the equation also contains a term that does not depend directly on the curvature, and is the force the electric field exerts on the surface charge. The form of the B_i's are summarized below:

$$B_1=\frac{4\pi^2h^2\sigma_0^2}{\bar{\epsilon}}\log k^{-1}, \tag{82}$$

$$B_2=\pi h^2(\beta+1)E_\infty\sigma_0 h\log k^{-1}, \tag{83}$$

$$B_3=-h\frac{\sigma_0^2\pi^2h^4}{\bar{\epsilon}}\log k^{-1}, \tag{84}$$

$$B_4=-\frac{\pi h^4\sigma_0^2 h}{K}\log k^{-1}. \tag{85}$$

The contribution to the tension (B_1) is negative and represents the self-repulsion effect denoted above. This instability is stabilized by B_3. Both the term B_2 and the term proportional to $\mathbf{E}_\infty\cdot\xi$ represents the interaction between the static charge density and the static electric field. Both of these forces are out of phase with the other terms. By themselves, these represent an oscillatory instability. Finally, the term B_4 competes with the viscous stabilization discussed above.

The consequences of including a static charge density are thus seen to be the following: (a) if the charge density is large enough that B_1 exceeds A_1, the jet is unstable. The growth rate of this instability is not small even when the conductivity is very large, in marked contrast to the case described above where there is no free charge. The instability can therefore be much more violent when significant free charge is present. (b) Surface charge fights against viscous stabilization. If the surface charge is large enough the instability will be peaked at high k, which signals the breakdown of the long wavelength theory (and a possible kinking of the jet). (c) If the normal electric field produced by the surface charge is of order the tangential field, the situation is complicated. Not only are all of the aforementioned effects acting, but there are also effects coupling the static surface charge to the tangential electric field (term B_2, and the normal force term). Both of these effects are out of phase with the others, and could themselves dominate if conditions were right.

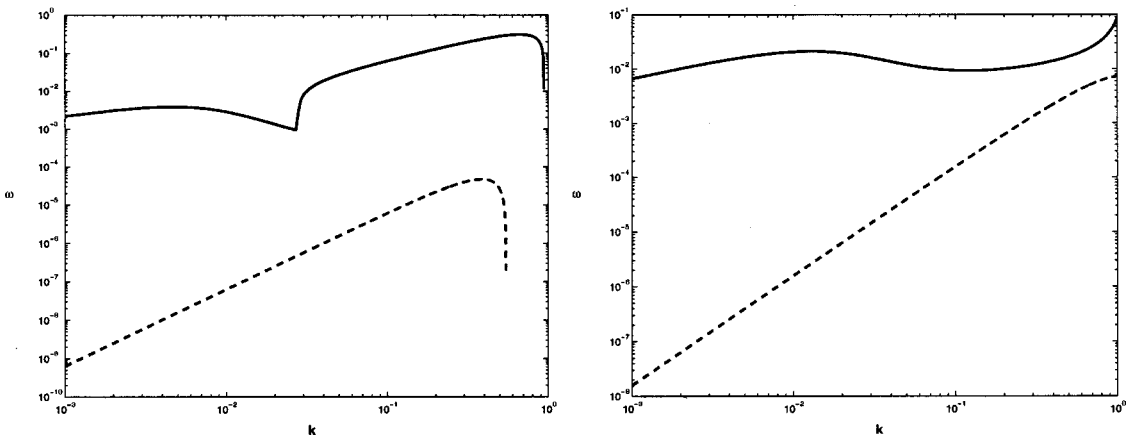

FIG. 19. Comparison of the axisymmetric mode (solid line) to the whipping mode (dashed line), for the conditions of Taylor's 1969 experiment except the jet has no surface charge, for two different field strengths, 1 kV/cm and 5 kV/cm (right). At 1 kV/cm both the Rayleigh and the axisymmetric conducting mode are stronger than the whipping mode. At 5 kV/cm the Rayleigh mode is suppressed but the axisymmetric conducting mode still dominates the whipping mode. This contradicts the primary observation from the experiment, where the whipping mode is observed to strongly dominate.

IV. COMPETITION BETWEEN WHIPPING MODE AND AXISYMMETRIC MODE

To summarize the results, we have identified three different instability modes of the jet: (1) the *Rayleigh mode*, which is the axisymmetric extension of the classical Rayleigh instability when electrical effects are important; (2) the *axisymmetric conducting mode*, and (3) the *whipping conducting mode*. (The latter are dubbed ''conducting modes'' because they only exist when the conductivity of the fluid is finite.) Whereas the classical Rayleigh instability is suppressed with increasing field and surface charge density, the conducting modes are enhanced. For this reason, at an appreciable field strength characteristic of experiments, the conducting modes dominate. The character of the whipping conducting mode depends strongly on whether the local electric field near the jet is dominated by its own static charge density (σ_0), or the tangential electric field E_∞. In the latter case, for a high conductivity fluid the instability is fairly suppressed (the growth rate is $O(K^{-1})$), whereas in the former it can be quite large. In general, the nature of the conducting instability that occurs strongly depends on the fluid parameters of the jet (viscosity, dielectric constant, conductivity).

In this section we analyze the competition between the axisymmetric and the whipping conducting modes as a function of parameters and determine where in parameter space each of them dominates. We will see that the dominant instability depends strongly on the static charge density of the jet. In the next paper we will determine what sets this charge density. Finally, we will put this all together in a way that is useful for deducing the implications for experiments.

To begin, we consider the competition between the various modes for Taylor's 1969 experiment,[29] which prompted Saville's original calculations. Taylor considered a jet of water emanating from a nozzle of 0.053 cm, under a range of electric fields from 1 kV/cm to ~5 kV/cm. Saville's analysis demonstrated that in the limit of zero viscosity and no surface charge density at sufficiently high fields the oscillatory whipping mode is more unstable than the axisymmetric instability; this result was consistent with Taylor's experiment,

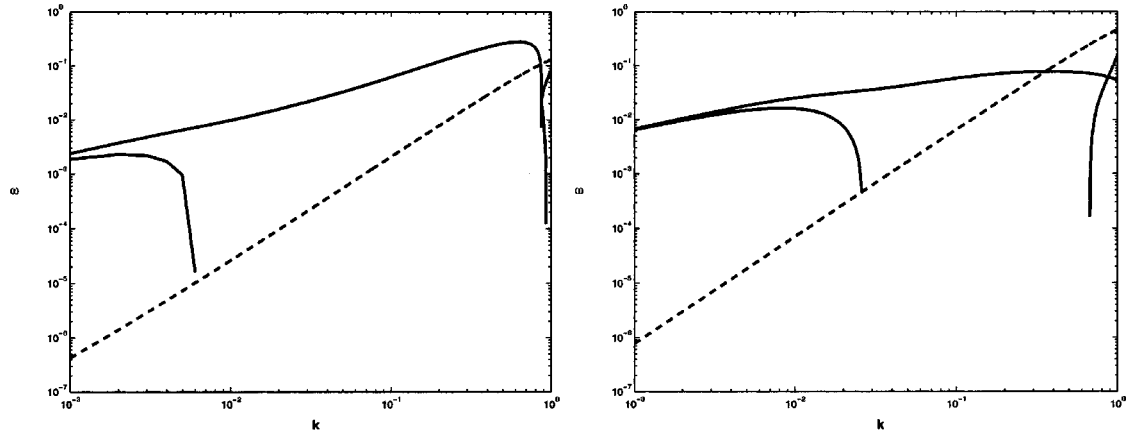

FIG. 20. Comparison of the axisymmetric modes (solid) to the whipping mode (dashed), for the same conditions as Fig. 19, except the jet has a small surface charge $\sigma_0 = 0.1$. At low fields, the axisymmetric modes still dominate the whipping mode; however at 5 kV/cm the whipping mode is stronger than both of the axisymmetric modes.

in that Taylor also observed that at fields above approximately 2 kV/cm the jet began to whip.

Figure 19 compares the two modes for a range of different field strengths; this figure is the same as Saville's comparison (i.e., surface charge is neglected), except that we are including the correct viscous effects as well. Interestingly, we find that when viscosity is included, the *ordering of the modes is reversed*: namely, the analysis predicts that the axisymmetric mode is much more unstable than the whipping mode; at an electric field of 5 kV/cm, the maximum growth rate of the whipping mode is four orders of magnitude lower than that for the axisymmetric mode! Based on the scaling arguments presented above, the reason for this is clear.

Including viscosity has two principal effects. First, it decreases the most unstable wavelength for the whipping mode to low wave numbers. Second, it switches the relative dominance of the axisymmetric and whipping modes. The first effect is consistent with the experiments, which observe a long wavelength instability. The second effect, however, contradicts experiments which clearly demonstrate a pronounced whipping instability.

The only ingredient available to resolve this conundrum is surface charge density. We now plot the same set of dispersion relations, but this time with an experimentally reasonable surface charge included. The surface charge corresponds to that which would be present if there were a current of a few nanoamperes passing through the jet (Fig. 20).

At low fields, both the axisymmetric modes are stronger than the whipping mode; at the highest field 5 kV/cm the whipping mode is stronger than both of the axisymmetric modes! The reason for this is that the electric field normal to the jet produced by the surface charge is actually slightly larger than the tangential electric field. For reasons that have been previously discussed in the electrospraying literature[21] and will be discussed in the second paper of this series, a small current passing through the jet results in a rather large surface charge. Hence, when *both* surface charge and viscosity are included, the stability analysis is qualitatively consistent with the experiments. To achieve quantitative agreement, it is necessary to determine quantitatively the surface charge along the jet.

Before closing this paper, we first summarize the competition between the axisymmetric and whipping modes through a phase diagram. This will be useful for interpreting experiments. Since both the surface charge density and the jet radius vary away from the nozzle, the stability characteristics of the jet will change as the jet thins. [The electric field also varies along the jet; however, in the plate–plate experimental geometry that we use (Fig. 1) the field everywhere along the jet is dominated by the externally applied field produced by the capacitor plates, so it is safe to neglect the field's variance. To apply the present results to experiments in the point–plate geometry, it would be necessary to include the variation of the field along the jet as well.] Figure 21 shows an illustrative result for a fluid with viscosity 16.7 P, conductivity 120 μS/cm in an external electric field 2 kV/cm. The phase diagram shows the logarithm of the ratio of the maximum growth rate of the whipping conducting mode to the maximum growth rate of all axisymmetric modes as a function of σ and h. We saturate this ratio at 2 and 1/2 so that the detail of the transition can be seen. In the light regions, a whipping mode is twice or more times as unstable as all axisymmetric modes; in the dark regions, the axisymmetric is more unstable. As anticipated from the arguments above, the whipping modes are more unstable for higher charge densities (to the right), whereas the axisymmetric modes dominate in the low charge density region (to the left).

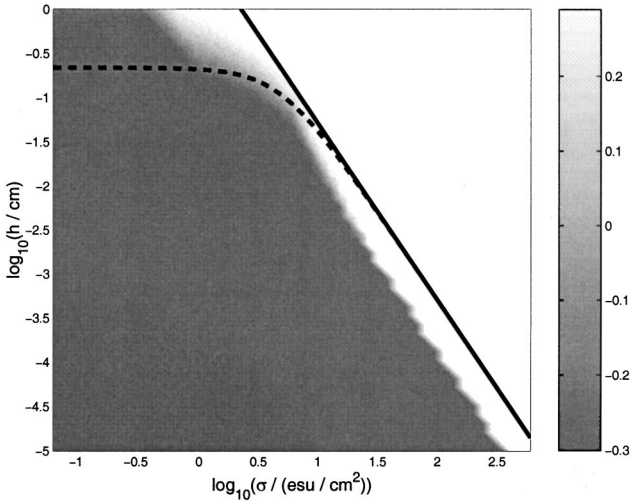

FIG. 21. Contour plot of the logarithm (base ten) of the ratio of the growth rate of the most unstable whipping mode to the most unstable varicose mode, for a polyetheleneoxide–water mixture ($\nu = 16.7\ \mathrm{cm}^2/\mathrm{s}$ and $K = 120\ \mu$S/cm). The ratio is cut off at 2 and 1/2 so that the detail of the transition can be seen. In all cases, the axisymmetric instability prevails at low charge density and the whipping dominates at high charge density. The solid line shows the borderline above, and to the right, of which the system is unstable to the Rayleigh whipping instability. The dashed line shows the borderline below and to the right of which the Rayleigh varicose instability is not suppressed.

The solid line in the figure shows the Rayleigh charge threshold for the whipping mode, when $A_1 = B_1$. To the left of the line, charge repulsion beats surface tension and thus causes instability. As seen in the figure, the whipping modes becomes dominant when the charge density is about an order of magnitude smaller than this threshold, because of the the interaction of the static charge density with the external electric field. The solid dashed line shows the curve above where the axisymmetric Rayleigh instability is suppressed $2\pi\sigma_0^2 + (4\pi)^{-1}\Omega_0^2 = 1/2$. Note that the axisymmetric Rayleigh instability mode is operative at low radii and low charge densities, while the whipping Rayleigh charge instability dominates at high radii and high charge densities. The combining of these two effects explains why whipping dominates at high charge density in high conductivity fluids. The growth rate of the conducting modes vanishes with increasing conductivity and thus when one of the classical (conductivity independent) Rayleigh modes is present, it dominates.

V. CONCLUSIONS

The main task of this paper has been performing a complete stability analysis of a charged fluid jet in a tangential electric field as a function of all fluid parameters. The stabil-

ity analysis relied on an asymptotic expansion of the equations of electrohydrodynamics in powers of the aspect ratio of the perturbations, which were assumed to be small. The analysis extends previous works to the parameter regimes important for experiments. The second paper in this series uses the stability analysis, in conjunction with an analysis of the charge distribution and radius of the jets in our electrospinning experiments, to derive quantitative thresholds for the onset of electrospinning as a function of all experimental parameters.

ACKNOWLEDGMENTS

We are grateful to L. P. Kadanoff, L. Mahadevan, D. Saville, and D. Reneker for useful conversations. We also thank A. Ganan Calvo for detailed comments and criticisms on the manuscript. M.M.H. acknowledges support from the MRSEC at the University of Chicago, as well as support from the NSF under Grant No. DMR 9718858. M.B. and M.M.H. gratefully acknowledge funding from the Donors of The Petroleum Research Fund, administered by the American Chemical Society, for partial support of this research; and also the NSF Division of Mathematical Sciences. M.S. and G.R. are grateful to the National Textile Center for funding this research project, No. M98-D01, under the United States Department of Commerce Grant No. 99-27-7400.

[1] J. Doshi and D. H. Reneker, ''Electrospinning process and applications of electrospun fibers,'' J. Electrost. **35**, 151 (1995).
[2] R. Jaeger, M. Bergshoef, C. Martin-Batille, H. Schoenherr, and G. J. Vansco, ''Electrospinning of ultrathin polymer fibers,'' Macromol. Symp. **127**, 141 (1998).
[3] P. Gibson, H. Schreuder-Gibson, and C. Pentheny, ''Electrospinning technology: Direct application of tailorable ultrathin membranes,'' J. Coated Fabr. **28**, 63 (1998).
[4] J. S. Kim and D. H. Reneker, ''Mechanical properties of composites using ultrafine electrospun fibers,'' Polym. Compos. **20**, 124 (1999).
[5] L. Huang, R. A. McMillan, R. P. Apkarian *et al.*, ''Generation of synthetic elastin-mimetic small diameter fibers and fiber networks,'' Macromolecules **33**, 2899 (2000).
[6] P. K. Baumgarten, ''Electrostatic spinning of acrylic microfibers,'' J. Colloid Interface Sci. **36**, 71 (1971).
[7] L. Larrondo and R. St. John Manley, ''Electrostatic fiber spinning from polymer melts (i): Experimental observation of fiber formation and properties,'' J. Polym. Sci., Polym. Phys. Ed. **19**, 909 (1981).
[8] M. Shin, M. M. Hohman, M. P. Brenner, and G. C. Rutledge, ''Electrospinning: A whipping fluid jet generates submicron polymer fibers,'' Appl. Phys. Lett. **78**, 1149 (2001).
[9] A. G. Bailey, *Electro-Static Spraying of Liquids* (Wiley, New York, 1988).
[10] B. Vonnegut and R. L. Neubauer, ''Production of monodisperse liquid particles by electrical atomization,'' J. Colloid Sci. **7**, 616 (1952).
[11] G. M. H. Meesters, P. H. W. Vercoulen, J. C. M. Marijnissen, and B. Scarlett, ''Generation of micron-sized droplets from the Taylor cone,'' J. Aerosol Sci. **23**, 37 (1992).
[12] A. Gomez and K. Tang, ''Charge and fission of droplets in electrostatic sprays,'' Phys. Fluids **6**, 404 (1994).
[13] K. Tang and A. Gomez, ''On the structure of an electrostatic spray of monodisperse droplets,'' Phys. Fluids **6**, 2317 (1994).
[14] J. Fernandez de la Mora, ''The effect of charge emission from electrified liquid cones,'' J. Fluid Mech. **243**, 561 (1992).
[15] M. Cloupeau and B. Prunet-Foch, ''Electrostatic spraying of liquids in cone-jet mode,'' J. Electrost. **22**, 135 (1989).
[16] M. Cloupeau and B. Prunet-Foch, ''Electrohydrodynamic spraying functioning modes: A critical review,'' J. Aerosol Sci. **25**, 1021 (1994).
[17] A. Jaworek and A. Krupa, ''Classification of the modes of end spraying,'' J. Aerosol Sci. **30**, 873 (1999).
[18] J. R. Melcher and E. P. Warren, ''Electrohydrodynamics of current carrying semi-insulating jet,'' J. Fluid Mech. **47**, 127 (1971).
[19] C. Pantano, A. M. Ganan-Calvo, and A. Barrero, ''Zeroth-order, electrohydrostatic solution for electrospraying in cone-jet mode,'' J. Aerosol Sci. **25**, 1065 (1994).
[20] A. M. Ganan-Calvo, J. Dávila, and A. Barrero, ''Current and droplet size in the electrospraying of liquids: Scaling laws,'' J. Aerosol Sci. **28**, 249 (1997).
[21] A. M. Ganan-Calvo, ''On the theory of electrohydrodynamically driven capillary jets,'' J. Fluid Mech. **335**, 165 (1997).
[22] A. M. Ganan-Calvo, ''Cone-jet analytical extension of Taylor's electrostatic solution and the asymptotic universal scaling laws in electrospraying,'' Phys. Rev. Lett. **79**, 217 (1997).
[23] I. Hayati, A. Bailey, and Th. Tadros, ''Investigations into the mechanism of electrohydrodynamic spraying of liquids,'' J. Colloid Interface Sci. **117**, 205 (1986).
[24] L. T. Cherney, ''Structure of Taylor cone-jets: Limit of low flow rates,'' J. Fluid Mech. **378**, 167 (1999).
[25] L. T. Cherney, ''Electrohydrodynamics of electrified liquid minisci and emitted jets,'' J. Aerosol Sci. **30**, 851 (1999).
[26] J. Fernàndez de la Mora and I. G. Loscertales, ''The current emitted by highly conducting Taylor cones,'' J. Fluid Mech. **260**, 155 (1994).
[27] G. I. Taylor, ''Disintegration of water drops in an electric field,'' Proc. R. Soc. London, Ser. A **280**, 383 (1964).
[28] G. I. Taylor, ''The circulation produced in a drop by an electric field,'' Proc. R. Soc. London **291**, 159 (1966).
[29] G. I. Taylor, ''Electrically driven jets,'' Proc. R. Soc. London, Ser. A **313**, 453 (1969).
[30] J. R. Melcher and G. I. Taylor, ''Electrohydrodynamics: A review of the role of interfacial shear stresses,'' Annu. Rev. Fluid Mech. **1**, 111 (1969).
[31] D. A. Saville, ''Electrohydrodynamics: The Taylor–Melcher leaky dielectric model,'' Annu. Rev. Fluid Mech. **29**, 27 (1997).
[32] D. A. Saville, ''Electrohydrodynamic stability: Fluid cylinders in longitudinal electric fields,'' Phys. Fluids **13**, 2987 (1970).
[33] D. A. Saville, ''Electrohydrodynamic stability: Effects of charge relaxation on the interface of a liquid jet,'' J. Fluid Mech. **48**, 815 (1971).
[34] D. A. Saville, ''Stability of electrically charged viscous cylinders,'' Phys. Fluids **14**, 1095 (1971).
[35] A. L. Huebner and H. N. Chu, ''Instability and breakup of charged liquid jets,'' J. Fluid Mech. **49**, 361 (1970).
[36] A. J. Mestel, ''Electrohydrodynamic stability of a slightly viscous jet,'' J. Fluid Mech. **274**, 93 (1994).
[37] A. J. Mestel, ''Electrohydrodynamic stability of a highly viscous jet,'' J. Fluid Mech. **312**, 311 (1996).
[38] J. Eggers, ''Nonlinear dynamics and breakup of free-surface flows,'' Rev. Mod. Phys. **69**, 865 (1997).
[39] H. A. Stone, J. R. Lister, and M. P. Brenner, ''Drops with conical ends in electric and magnetic fields,'' Proc. R. Soc. London, Ser. A **455**, 329 (1999).
[40] L. Landau and L. Lifshitz, *Theory of Elasticity* (Addison–Wesley, Reading, 1959).
[41] J. M. Lopez-Herrera, A. M. Ganan-Calvo, and M. Perez-Saborid, ''One dimensional simulation of the breakup of capillary jets of conducting liquids: Application to e.h.d. spraying,'' J. Aerosol Sci. **30**, 895 (1999).
[42] M. Shin, M. M. Hohman, M. P. Brenner, and G. C. Rutledge, ''Experimental characterization of electrospinning,'' Polymer (submitted).
[43] L. Mahadevan, W. S. Ryu, and A. D. T. Samuel, ''Fluid rope trick revisited,'' Nature (London) **392**, 140 (1998).
[44] R. da Silveira, S. Chaieb, and L. Mahadevan, ''Rippling instability of a collapsing bubble,'' Science **287**, 1468 (2000).